P450cam (CYP101A1) Mutants for Endosulfan Degradation: Complete Dehalogenation of Endosulfan Diol and Related Compounds

Abdul Rehman
Simon Fraser University
Nicole Gkaleni
Simon Fraser University
Priyadarshini Balaraman
Simon Fraser University
Brinda Prasad
Simon Fraser University
Erika Plettner (plettner@sfu.ca)
Simon Fraser University

Research Article

Keywords: Cytochrome P450cam, dehalogenation, Endosulfan biodegradation, Heptachlor, Oxidation

Posted Date: June 17th, 2022

DOI: https://doi.org/10.21203/rs.3.rs-1759048/v1

$P450_{cam}$ (CYP101A1) Mutants for Endosulfan Degradation: Complete Dehalogenation of Endosulfan Diol and Related Compounds

*Abdul Rehman,[a] Nicole Gkaleni,[a] Priyadarshini Balaraman,[a] Brinda Prasad, [ab] Erika Plettner.[a]**

[a] Department of Chemistry, Simon Fraser University, 8888 Univ. Dr., Burnaby, B. C. V5A 1S6, Canada

[b] Currently working as a consultant in Germany

[*] Author for correspondence

e-mail: plettner@sfu.ca

Tel.: 778-782-3586

FAX 778-782-3765

Abstract: Cytochrome $P450_{cam}$ (CYP101A1) from the soil bacterium *Pseudomonas putida* oxidizes camphor regio- and stereoselectively at the 5-position, to give 5-*exo*-hydroxycamphor. Previously, we randomly mutated $P450_{cam}$ and selected seven mutants on the bicyclic polychlorinated insecticide and persistent organic pollutant, endosulfan (ES). Here we describe the activity of the seven mutants of $P450_{cam}$ with ES diol, ES, ES lactone, ES ether, ES sulfate, and heptachlor. ES diol, ES lactone, ES ether, and ES sulfate are persistent biotransformation products of ES in the environment. They all have the hexachlorinated norbornene (bicyclo[2.2.1] hept-2-ene) moiety intact. The $P450_{cam}$ mutants (and to a small extent the wild type) convert these substrates to substituted *ortho*-quinones, which we detected using 4-aminoantipyrine (4-AAP) in spectrophotometric assays. Here we have studied dehalogenation of ES and related compounds catalyzed by the endosulfan–selected $P450_{cam}$ mutants, using *in vitro* kinetics, chloride release assays, and ^{13}C labeled endosulfan diol. We found that mutants *ES*7 (V247F/D297N/K314E) and *ES*6 (G120S) were significantly more active towards ES diol than the WT. On average, close to six Cl^- ions are released per aromatic product detected upon turnover of ES diol. Finally, product isolation from reactions with non-labeled and ^{13}C labeled ES diol confirmed that substituted catechols formed. Based on these findings, we propose that dehalogenagion begins with the oxidation of the ES double bond on the norbornene system, proceeds with eliminating six chloride ions and loss of the bridge as CO_2 to furnish an *ortho*-quinone, which can be reduced non-enzymatically to the corresponding catechol.

KEYWORDS. Cytochrome $P450_{cam}$, dehalogenation, Endosulfan biodegradation, Heptachlor, Oxidation.

Introduction

Many organic chlorinated compounds were introduced as insecticides in the 1950s, including bicyclic compounds such as endosulfan (ES, **1**) and heptachlor (HC, **2**). Endosulfan **1**, a hexachlorinated compound, is effective against a broad range of insects and mites, which caused ES to be used widely on a variety of crops, such as: cotton, cereals, potatoes, spinach, coffee, tea, pome fruit and berries (reviewed: (Rehman 2021)).

ES exists as two diastereomers: α-endosulfan and β-endosulfan (**Fig. 1**) (Schmidt et al. 1997, Schmidt et al. 2001). Technical grade ES is a mixture of these two isomers, ranging from 2:1 to 7:3 (α:β). ES has a long half-life in soil (α-ES 35 – 37 days and β-ES 104 – 265 days) and is, therefore, persistent in the environment (Jimenez-Torres et al. 2016). ES accumulates in marine environments and is toxic to fish, algae, and other marine life (reviewed: (Rehman 2021)). In addition, ES shows human neurotoxicity (Enhui, Na et al. 2016), affects estrogen and androgen receptors in females, and delays male reproductive development (reviewed: (Rehman 2021)). ES and its metabolites have adverse effects on babies and can cause acute toxicity and death after ingestion (Dawson et al. 2010). ES is harmful to beneficial insects such as honey bees (Stanley et al. 2015).

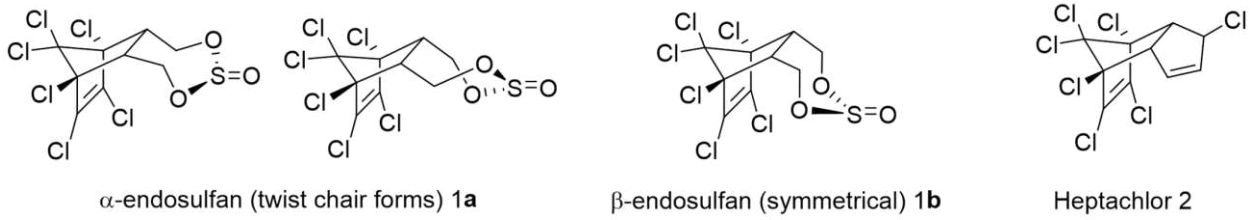

Fig. 1 Structures of the endosulfan (ES, **1**) diastereoisomers, known as α-ES (**1a**) and β-ES (**1b**), and structure of heptachlor (HC, **2**)

ES is persistent in the environment and has been accumulating in the food chain (Kelly et al. 2007) due to its hydrophobicity (log K_{ow}α 4.74 and log K_{ow}β 4.78) (Shen and Wania 2005, Shen

et al. 2005). Also, through transport in the atmosphere, ES has been found as far south as Antarctica and as far north as the Arctic ocean (Pozo et al. 2006, Weber et al. 2006, Kelly et al. 2007, Luek et al. 2017). According to the Stockholm Convention, ES is classified as a 'Persistent Organic Pollutant. In 2011, 80 countries agreed to ban ES, and its use was phased out in the United States and Canada in 2016 (review: (Rehman 2021)).

Heptachlor (HC, **2**) was first isolated from technical chlordane in 1946 and was mostly used during the 1960s and 1970s by exterminators against termites. Most of its applications were banned during the 1980s in many countries, and the Stockholm treaty restricted its use in 2001 to underground cable boxes and as a termiticide in power transformers (reviewed: (Gkaleni 2021)).

Technical grade HC contains ~72% heptachlor and ~28% related compounds, such as *trans*-chlordane (~20%) and *trans*-nonachlor (up to 8%). Due to its hydrophobicity (log K_{ow} 3.87-5.44), HC has a long half-life in soil (up to 2 years), so it is persistent in the environment and accumulates in the food chain (reviewed: (Gkaleni 2021)). HC is toxic towards aquatic life, including algae, plankton, invertebrates, and fish (Fendick, Mather-Mihaich et al. 1990). HC shows immunotoxic and neurotoxicological effects, and it increases the risk of breast cancer, because it accumulates in adipose tissues in humans (reviewed: (Gkaleni 2021)).

Since both ES (**1**) and HC (**2**) are persistent in the environment, their transformation pathways have been studied. ES has a sulfite ester moiety that can be oxidized to sulfate (**Fig. 2**). Hydrolysis of ES sulfate (**9**) in alkaline conditions (for example, seawater) results in formation of ES diol (**3**) (Kullman and Matsumura 1996). In soil and aquatic environments, ES sulfate and ES diol are two metabolites found along with ES (**Fig. 2a**) (Harman-Fetcho et al. 2005, Wan et al. 2006). Other metabolites formed by biodegradation of ES are: ES lactone (**4**), ES ether (**5**), ES hemiacetal (**6**), ES monoaldehyde (**7**), and dialdehyde (**8**), among others (**Fig. 2a**) (Sutherland et al. 2000, Kwon

et al. 2002, Sutherland et al. 2002, Sutherland et al. 2002, Sutherland et al. 2002, Walse et al. 2003, Hussain et al. 2007, Hussain et al. 2007, Kataoka et al. 2010, Kataoka et al. 2011).

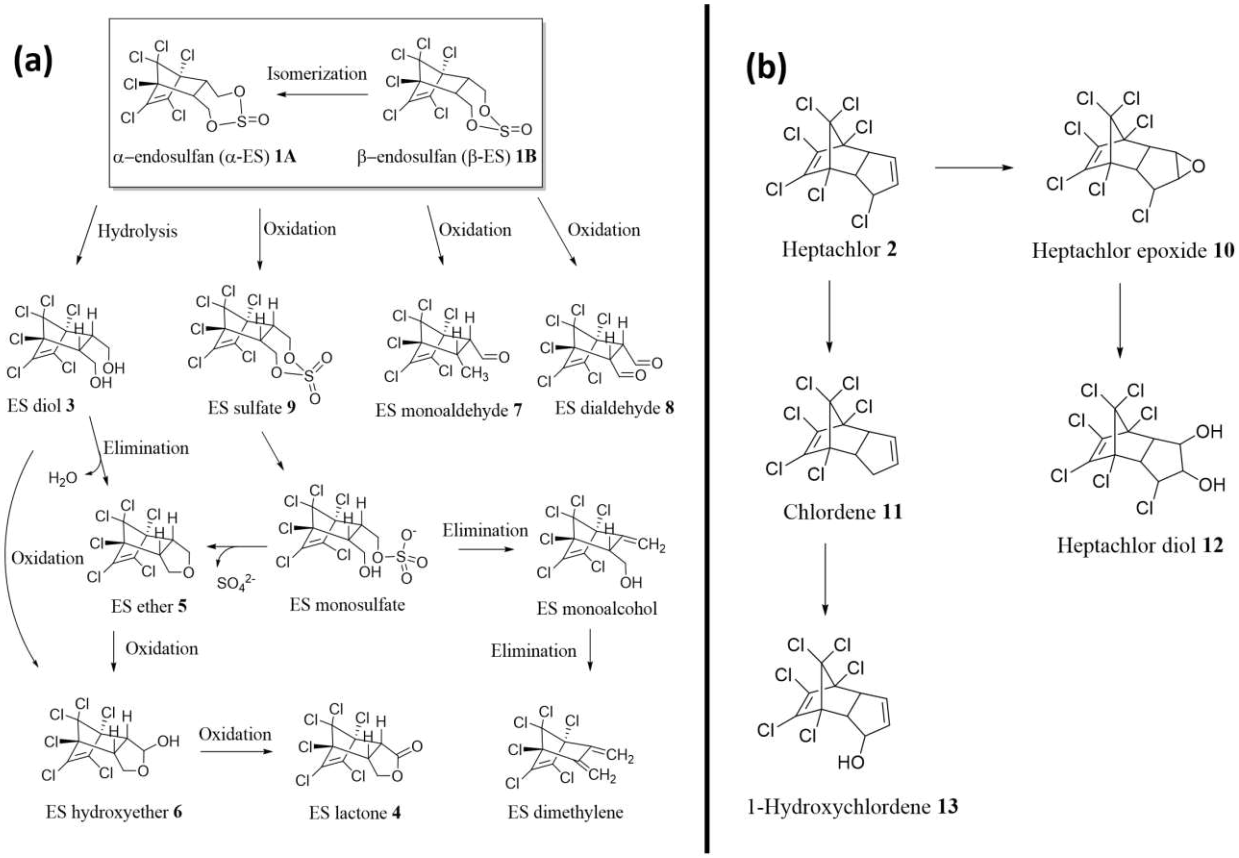

Fig. 2 Known ES (**a**) and HC (**b**) metabolites found in the environment. Note that they all have the hexachloronorbornene moiety intact

HC can be transformed by abiotic processes and may undergo photolysis, oxidation, and volatilization. It can also be transformed biologically to HC epoxide (**10**), which is more persistent and toxic than HC (Wauchope et al. 1992). Miles et al. (Miles et al. 1969, Miles et al. 1971) were the first to provide evidence of HC degradation by soil microorganisms. According to their studies, several fungi, bacteria, and actinomycetes were shown to metabolize HC by epoxidation, hydrolysis, and reduction pathways. HC's chloro-cyclopentene moiety can be epoxidized to heptachlor epoxide (**10**) (**Fig. 2b**). In aquatic environments, hydrolysis of the epoxide moiety

results in HC diol (**12**). Lastly, HC can also get dechlorinated to chlordene (**11**) and then hydroxylated to 1-hydroxychlordene (**13**).

Since the known ES (**1**) and HC (**2**) biodegradation pathways only target the oxidation and/or elimination from the non-chlorinated part of the molecule retaining the six chlorine atoms intact on the bicyclic core, the known metabolites of ES and HC are still hydrophobic and accumulate in the environment (**Fig. 2**). Therefore, dechlorination of ES, HC, and/or its metabolites is highly desirable but still unknown in the known biodegradation systems of these compounds. Here we describe some mutants of cytochrome $P450_{cam}$ (CYP101A1) that are capable of dechlorinating ES (**1**), ES diol (**3**), ES lactone (**4**), ES ether (**5**), and HC (**2**).

Cytochromes P450 (P450s) are heme-containing monooxygenases known to insert oxygen into C-H bonds (Ortiz de Montellano 2015). Other reactions catalyzed by cytochromes P450 are epoxidation, sulfur oxidation, N- and O-dealkylation, and many others (Cryle and Voss 2006). Mutations to the active site of cytochromes P450 can lead to an increased substrate range and/or altered catalytic activity of the enzyme. Cytochrome $P450_{cam}$ (CYP101A1) from the soil bacterium *Pseudomonas putida* ATCC 17453 oxidizes camphor regio- and stereoselectively at the 5-position, to give 5-*exo*-hydroxycamphor, and after double oxidation to 5-ketocamphor (Auclair et al. 2001, Prasad et al. 2011). Wild-type $P450_{cam}$ is also reported to catalyze the reductive dehalogenation of chlorinated compounds like hexachloroethane, pentachloroethane, 1,1,1,2-tetrachloroethane, and 1,1,1-trichlorotrifluoroethane to the respective metabolites, tetrachlorothene, trichloroethene, 1,1-dichloroethene and dichlorodifluoromethane, under low oxygen concentration (Li and Wackett 1993, Wackett et al. 1994, Wackett 1995). Hepatic cytochromes P450 have been reported to oxidize vinylidene chloride, yielding 2,2-dichloroacetaldehyde or 2-chloroacetic acid as products (Liebler and Guengerich 1983). However, to our knowledge, there are no reports of dehalogenation

studies on larger polychlorinated substrates, such as ES (**1**) or HC (**2**). In the present paper, we report on $P450_{cam}$ mutants that can oxidatively dechlorinate ES, HC and several ES metabolites.

In our previous work, we generated a library of $P450_{cam}$ mutants by Sequence Saturation Mutagenesis (SeSaM) (Kammoonah et al. 2018), transformed the library into an expression host, and selected it on minimal media containing technical ES (**1**) as a sole carbon source and at a level that was found to be toxic to the expression host. We have identified seven mutants of $P450_{cam}$ that can convert ES diol (**3**) and ES lactone (**4**), into dechlorinated products (substituted *o*-quinones and/or catechols). Due to difficulty in isolating/detecting these product(s), we coupled them in the assay to 4-aminoantipyrine (4-AAP, **14**), to give a colored polar adduct (**Fig. 3**). We describe the relative activity of these mutants using the coupled assay, and we interpret the activity in terms of the mutations and the predicted ability of the mutant enzymes to position the double bond of the endosulfan substrates above the heme iron. We propose a plausible route by which the six chlorine atoms could be lost after oxidation of the double bond, based on chloride release data and experiments with ^{13}C labeled ES diol. We also studied the dechlorination of HC (**2**) and of major known ES metabolites by the most stable and active mutants using the coupled 4-AAP assay.

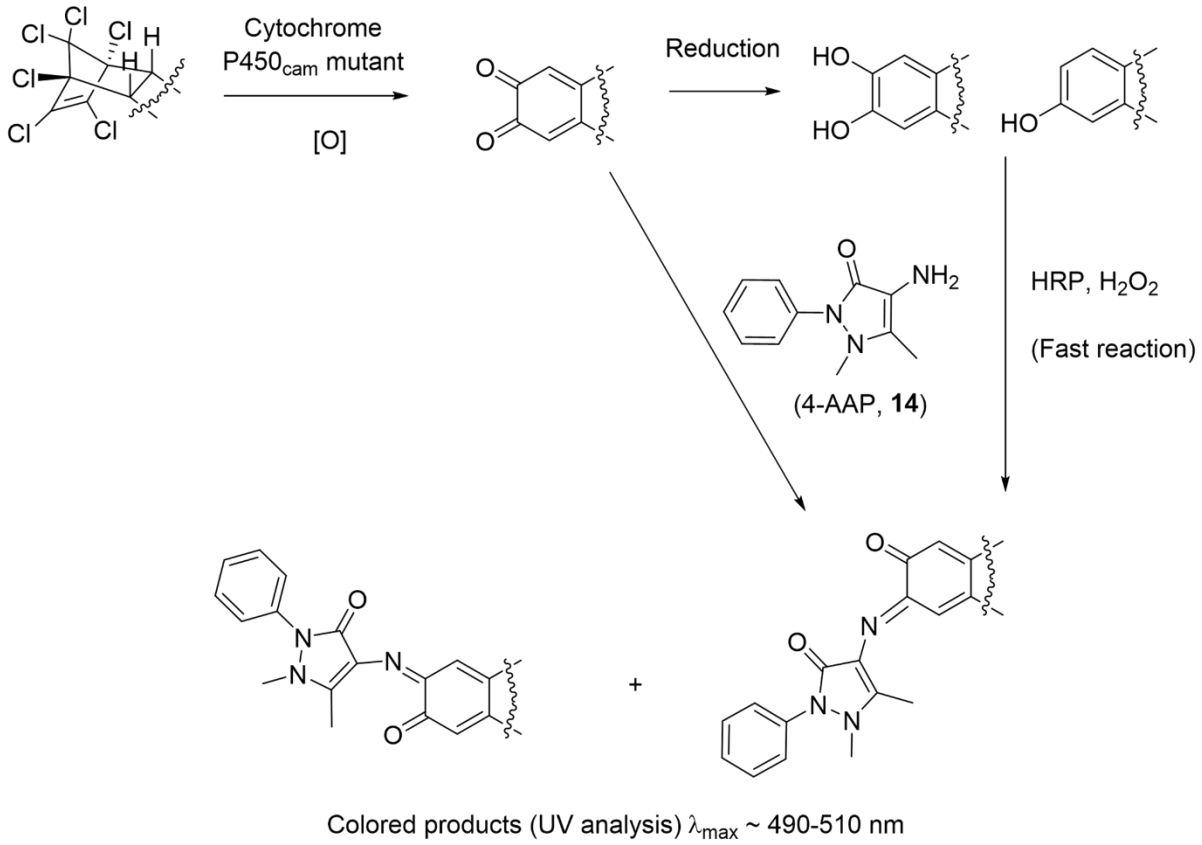

Fig. 3 Detection of the metabolites formed from ES or HC substrates in a coupled assay with 4-aminoantipyrine (4-AAP, **14**). The P450 is proposed to produce *ortho*-quinones (see below) which can be reduced to phenols non enzymatically. The latter are reoxidized by horseradish peroxidase (HRP) and H_2O_2, and the combined *o*-quinone is derivatized with 4-AAP, to give a colored product

Materials and methods

General Methods

Chemicals were of analytical grade and purchased from Sigma-Aldrich Canada (Oakville, Ontario). *m*-chloroperbenzoic acid (*m*-CPBA), endosulfan (a 2:1 mixture of α and β isomers commonly used) and 1,4,5,6,7,7-hexachloro-5-norbornene-2,3-dicarboxylic anhydride (chlorendic anhydride), 4-aminoantipyrine (4-AAP), and Peroxidase from Horseradish (Type VI,

HRP) were purchased from Sigma-Aldrich (Oakville, ON, Canada). *m*-CPBA was purified by reported methods (Armarego and Perrin 1997). Solvent evaporations were done on a Buchi Rotavapor (R-200), connected to a liquid nitrogen trap, and a laboratory vacuum (Piab® LVH40VK) system. Centrifugations were carried out with a Beckmann Avanti J-26 XPI centrifuge (Mississauga, ON, Canada), equipped with JLA 8.1000 and JA 25.50 rotors. NMR spectra were obtained using Bruker AVANCE II 400 MHz and/or 600 MHz instruments. Chloride ion release was measured using an Orion TM Chloride Electrode (9417BN) by Thermo Scientific (Ottawa, ON, Canada). Gas chromatography-mass spectrometry (GC-MS) was performed on either a Varian Saturn CP3800 GC, fitted with a 30 m SPB5 column (0.2 μm film thickness, 0.25 mm internal diameter, Supelco, USA) and interfaced with a Saturn 2000 ion trap mass spectrometer (MS), or on a Perkin Elmer Clarus 690 GC interfaced with a SQ8T MS, fitted with the same type of column as the Varian. The GC oven was programmed as follows: 45 ºC for 30 s; 7 ºC/min to 120 ºC, held for 1 min; then 50 ºC/min to 260 ºC, held 15 min. The ion trap mass detector was used in electron impact (EI, 70 eV) mode and fully scanned over a range of m/z 50-550. Acidified silica (silica Gel 60, 23-400 mesh) was prepared by adding it into H_3PO_4 (1 ml per 100 g of Silica) solution in methanol followed by decanting methanol and evaporation of residual methanol using a Rotavapor inside a fume hood.

Site-directed mutagenesis of WT $P450_{cam}$ was performed using the QuikChange Lightning Site-Directed Mutagenesis Kit (Agilent, Santa Clara, California, US). Primers for mutations were obtained from Integrated DNA Technologies, Inc. (Coralville, Iowa, US), and sequencing was done by Eurofins Genomics (Louisville, KY, US). Primers are listed in **Table S1**.

Synthesis of substrates and standards

Details of the syntheses are in the Supplemental Information. Briefly, ES lactone (**4**) was prepared from chlorendic anhydride by reduction with $NaBH_4$ in THF. ES diol (**3**) was prepared from lactone **4** by reduction with $LiAlH_4$ in THF. ES diol labeled with ^{13}C at positions 5 and 6 was prepared by reaction of hexachlorocyclopentadiene with 2,3-^{13}C maleic acid, to give labeled chlorendic acid. This was converted to chlorendic anhydride by reaction with acetyl chloride. The anhydride was reduced with $LiAlH_4$ to furnish the diol (**Scheme S1**). Compound **15**, 5,6-dimethoxy-2-benzofuran-1(3H)-one, was prepared from 3,4-dimethoxybenzoic acid by reaction with formaldehyde. Compound **16**, 5,6-dihydroxy-2-benzofuran-1(3H)-one, was prepared from **15** by removal of the methyl groups with BBr_3 in CH_2Cl_2. Compound **17**, the 4-AAP adduct of **16**, was prepared by reacting **16** with H_2O_2, HRP and 4-AAP.

Molecular biology methods

Initial experiments were done with a strain of *E. coli* BL21(DE3) that contained the originally selected clone of P450 (Kammoonah et al. 2018) and a bicistronic construct that contained both PdR and PdX (see supplemental information for the preparation of this strain and expression of the proteins).

Site-directed mutations of WT $P450_{cam}$ for His_6 – tagged $P450_{cam}$ mutant protein expression

Neither the WT nor the mutants we used in the previous section had a cleavable purification tag. Therefore, to facilitate expression and purification of the P450 mutants, we performed site-directed mutagenesis on the WT $P450_{cam}$ plasmid (pET-30 Xa/LIC), using 'QuikChange Lightning Multi Site-Directed Mutagenesis Kit (Agilent)' according to instructions. In summary, ds DNA WT $P450_{cam}$ plasmid template (isolated using Qiagen's QIAprep® Spin miniprep) was used. Using

'QuikChange Lightning Multi Site-Directed Mutagenesis Kit' components: 10 × QuikChange lightning multi reaction buffer (2.5 µL), Quik Solution (0.6 µL), ds DNA WT $P450_{cam}$ (100 ng), mutagenic primers (100 ng each primer, see primers list **Table S1**), dNTP mix (1 µL), QuikChange Lightning Multi enzyme blend (1 µL) and dd H_2O (to make total 25 µL). The PCR program was: 1 cycle of denaturation at 95 °C for 3 min, followed by 30 cycles of 95 °C (1.5 min), 55 °C (1 min), and 65 °C (12 min). The final extension was at 65 °C for 5 min. The resulting amplified product was treated with Dpn I restriction enzyme to digest the parent DNA strand (37 °C for 5 min).

Dpn I treated DNA (1.5 µL) was transformed into XL 10-Gold ultracompetent cells (pre-chilled, 45 µL) on ice (30 min) followed by heat-pulse at 42 °C (40 seconds). After incubating on ice (2 min), 0.5 mL of NYZ^+ broth was added and incubated at 37 °C (1 hour). This culture (50 µL) was plated on LB–agar plates (kanamycin 30 mg/L) and incubated overnight at 37 °C. A single colony was transferred to SOC media (kanamycin 30 mg/L) and incubated at 37 °C and 200 rpm overnight. The overnight grown culture was used to isolate DNA using Qiagen (QIAprep® Spin miniprep) kit following the instructions. DNA was sequenced (Eurofins Genomics, Louisville, KY) to verify the mutations (**Fig. S1-S7**). The isolated plasmid was then transferred to *E. coli* BL21(DE3) competent cells (Novagen, EMD Millipore Sigma, Etobicoke, Ontario, Canada) using the heat-shock method as described earlier.

WT $P450_{cam}$ and $P450_{cam}$ mutants (His_6 tagged) protein expression and purification

Each *E. coli* BL21(DE3) strain containing either WT $P450_{cam}$ or $P450_{cam}$ mutant (*ES*2, *ES*5, *ES*6 and *ES*7) plasmid was expressed as described. Induced cultures were harvested, and cells were lysed as described above. The crude lysate was dialyzed against phosphate buffer (50 mM

potassium phosphate buffer, pH 7.4 with 200 mM KCl) overnight using 3.5 KDa (MWCO) dialysis tubing (D304, Biodesign Dialysis tubing®, NY). The dialysate was purified using Nickel affinity column (Ni^{+2}) loaded with His-Bind resin® (Novagen) and eluted with increasing imidazole concentrations (3 – 25 mM) in phosphate buffer (50 mM potassium phosphate buffer, pH 7.4 with 200 mM KCl). Fractions with $P450_{cam}$ (analyzed by UV-Vis and SDS Page) were pooled and dialyzed against Tris buffer (4 L, 20 mM Tris buffer, pH 7.4 with 50 mM KCl and 1 mM $CaCl_2$) to remove imidazole before His_6 tag cleavage. The His-tag was cleaved using Factor Xa protease (Novagen) by adding 10 µL of enzyme per 2 mg of protein and incubating at room temperature for 36 – 48 hours. Factor Xa enzyme was removed by Xarrest ™ Agarose (Novagen), and His_6 tag fragment was removed by Nickel affinity column (Ni^{+2}) loaded with His-Bind resin®. Purified $P450_{cam}$ protein was analyzed by SDS Page (**Fig. S8**) and UV-Visible spectroscopy (see below) before kinetic studies.

Assays and spectroscopy of P450 enzymes

Analysis of protein samples for P450 concentration

The concentration of P450 in each crude lysate of $P450_{cam}$ mutants and WT $P450_{cam}$ was measured by UV analysis (at 418 nm for mutants $P450_{cam}$ and WT $P450_{cam}$) as described previously (Kammoonah et al. 2018). In addition, the purified and Factor Xa cleaved P450 mutants and WT were also analyzed by CO difference spectroscopy. The UV (400-500nm) spectra of oxidized $P450_{cam}$ mutants and WT $P450_{cam}$ were recorded in phosphate buffer (50 mM potassium phosphate buffer, pH 7.4 with 200 mM KCl). CO gas was bubbled for 2 minutes (~ 1 bubble per second), followed by the addition of sodium dithionite ($Na_2S_2O_4$, few grains) to reduce the P450 heme iron.

UV spectra were recorded again (400-500 nm) to see the Fe-CO peak at 450 nm (see supplementary data **Fig. S9**).

*Steady-state kinetic assays for endosulfan diol (ES diol **3**) with the crude lysates of $P450_{cam}$ mutant(s) using 4-aminoantipyrine (4-AAP, **14**) coupled assay with horseradish peroxidase (HRP) and H_2O_2*

Steady-state kinetic assays were performed in 1 mL potassium phosphate buffer (50 mM potassium phosphate, 200 mM KCl, pH 7.4) with varying concentrations of endosulfan diol (50 µM to 500 µM), 5 µM of crude protein $P450_{cam}$ mutant, NADH (800 µM), horseradish peroxidase (HRP, 1 unit/ml), H_2O_2 (30 % solution, 0.4 µl per ml) and 4-aminoantipyrine (4-AAP **14**, 2 mM). The reaction mixtures were monitored by UV-Visible spectroscopy for 3 and/or 20 minutes at 506 nm. Three controls were run in parallel: 1) in the absence of the substrate, 2) without HRP, or 3) without $P450_{cam}$. The kinetic assay was performed by first adding the phosphate buffer, 4-AAP, H_2O_2, NADH, HRP, and $P450_{cam}$ mutant protein, then adding the substrate (α-ES/ ES diol) and recording the absorbance at 506 nm. The assay was calibrated using 5,6-dihydroxy-2-benzofuran-1(3H)-one (**17**) at known concentrations, ranging from 10 µM to 300 µM, prepared under the same conditions as the enzymatic assay.

The initial detected amount of product formed was divided by 15 s, the time it took to insert the cuvette in the holder and start the monitoring of the reaction, to obtain the initial rates. The reason for doing this was that there was a rapid burst of activity, followed by a flattened progress curve (see **Fig. 4c**). In many cases, the progress curve was already flattening by the time absorbance at 506 nm was detected. Thus, the kinetic data for these experiments correspond to a 15 s endpoint and not the true initial rate.

For assays, 1 μ M of purified $P450_{cam}$ mutants (K314E, *ES*6 and *ES*7) or WT $P450_{cam}$ and pure redox partners PdX (3 μM), and PdR (3 μM) were used. Otherwise, the assay was the same as for the crude lysates.

To obtain the true initial rate (not the endpoint), a lower amount of purified *ES*7 (0.5 μM, instead of 1 μM), and a higher amount of PdX (6 μM instead of 3 μM) was used. PdR was as before (3 μM), with varying concentrations of endosulfan diol (50 μM to 500 μM). In addition, NADH, HRP, H_2O_2, and 4-AAP were used in the same concentrations as described above. The reaction mixtures were monitored by UV-Visible spectroscopy for 3 minutes at 506 nm. The rate of product formation was recorded over 3 minutes to obtain the initial rates. Initial rates were obtained by fitting the linear portion of the progress curves to a line ($R^2 \geq 0.98$) (**Fig. 5**).

Kinetic comparison of mutants ES*6 and* ES*7 with various substrates (ES diol, ES lactone, ES α:β, ES ether, ES sulfate, and heptachlor) using 4-aminoantipyrine (4-AAP,* ***14****) coupled assay with horseradish peroxidase (HRP) and* H_2O_2

The assay reaction mixture was a freshly prepared solution of phosphate buffer (50 mM potassium phosphate, 200 mM KCl, pH 7.4) containing 1 mM H_2O_2 (from a 37 % solution) and 2 mM 4-AAP, along with final concentrations of 2.2 μg HRP (1 unit per ml stock), 1.68 mM NADH, 1 μM of purified $P450_{cam}$ mutants (*ES*6 and *ES*7), 8 μM PdX, 2 μM PdR and the desired substrate (diluted in ethanol) in concentrations of 100 μM, 200 μM and 500 μM. The final volume of the assay was 500 μL, and the absorbance was monitored by UV-Visible spectroscopy at 506 nm for 3 minutes until a stable value was reached. The assays were performed by mixing all the materials, excluding the substrate, blanking the spectrophotometer, and then adding the substrate to record the absorbance. Three controls were run: 1) without the substrate, 2) without the enzyme, or 3)

without the substrate and the enzyme. The colorimetric reaction was calibrated by using 5,6-dihydroxy-2-benzofuran-1(3H)-one **17** (see the previous section). All assays were done in triplicate. Student's t-test was also carried out between the mutants and the WT enzyme to find the significant difference ($p < 0.05$).

*Titration of purified $P450_{cam}$ mutants with endosulfan diol (ES diol, **3**) and (+)-camphor, and dissociation constant (K_d)*

Purified $P450_{cam}$ mutant proteins (3 μM) were prepared in phosphate buffer (50 mM potassium phosphate buffer, pH 7.4 with 200 mM KCl). ES diol (2.5 μM - 250 μM) and (+)-camphor (1 μM - 50 μM) were added in aliquots using a Hamilton syringe, and UV-Visible spectra were recoded (350-500 nm, **Fig. 8**).

The total change in absorbance (ΔA) at 417 nm (substrate-free) and 390 nm (substrate-bound) was plotted against the concentration of substrate added, and this was used to calculate the dissociation constant (K_d) using a single-site binding model in GraphPad Prism® (GraphPad Software Inc. CA).

$$\Delta A = (\Delta A_{390}) + (\Delta A_{417})$$

*Chloride release from Endosulfan diol (**3**) with ES7, PdX, PdR and a NADH regeneration system*

The assay was performed in 5 mL potassium phosphate buffer (100 mM potassium phosphate, pH 7.4) with ES diol (**3**) (300 μM or 500 μM), purified WT-$P450_{cam}$ or ES7 mutant (1 μM), purified redox partners PdX (5 μM), and PdR (1 μM), NADH (500 μM), and alcohol dehydrogenase (350 units). Chloride (Cl^-) ion concentrations were measured using a chloride ion-selective electrode (chloride ISE) before and after adding ES diol (**3**). In addition, samples (1 ml) were taken before

and after adding ES diol (**3**), and 4-AAP (**14**) coupled assay with HRP and H_2O_2 were performed as described above. To measure the interference with chloride readings, control experiments were performed using sodium chloride solutions of known concentration and addition of 1) NADH or 2) NAD^+.

*Chloride release from Endosulfan diol (**3**) with ES7 and* m-*CPBA as a shunt*

The assay was performed in the same manner as described above, except that *m*-CPBA (1 mM) was added to purified WT-$P450_{cam}$ or *ES*7 mutant (5 μM), instead of PdX, PdR and NADH. To measure interference with chloride reading control experiments were performed using sodium chloride solutions of known concentration and addition of 1) *m*-CPBA and 2) chlorobenzoic acid.

At the end of the assay, the organic products were extracted with ethyl acetate (3 × 100 ml) and dried with Na_2SO_4. The solvent was evaporated, and the crude extract was analyzed by ^1H NMR and LC-MS (see Supplemental Information).

Assay with ES lactone and GC-MS identification of the product

The assay mixture contained 50 mM potassium phosphate buffer with 200 mM KCl (pH 7.4), 1 μM *ES*7, 1 μM PdR, 10 μM PdX, and 200 μM ES lactone. The reaction was initiated by the addition of 700 μM NADH and reacted overnight at room temperature. The aqueous solution was evaporated thoroughly in a vacuum concentrator and 5 drops of the BF_3·methanol reagent (0.1 mL of $BF_3.Et_2O$ in 1 mL of MeOH) were added and reacted overnight at room temperature in a sealed vial in an anaerobic chamber. Saturated solution of sodium bicarbonate was added until the bubbling seized. The aqueous solution was again evaporated thoroughly in a vacuum concentrator

followed by the addition of 10 µL chloroform and analyzed by GC-MS. Three controls were run in parallel: No substrate, no enzyme, and no NADH.

In silico docking studies

Docking simulations were performed using Molecular Operating Environment (MOE, Chemical Computing Group, Montreal, QC Canada). The amino acids and 3D structure information of $P450_{cam}$ (CYP101A1) were obtained from Protein Data Bank. $P450_{cam}$ with PDB code 2L8M (Reduced and CO-bond in the presence of camphor) was used for docking studies (Asciutto et al. 2011). The protein PDB file was imported to MOE, and residues were mutated to generate the $P450_{cam}$ mutants (*ES1-ES7, IND1, and K314E*). The preparation of the proteins for docking was performed as described by Kammoonah et al. (2018). In summary, camphor and carbon monoxide molecules were removed from the PDB structure. Each residue of the protein was protonated at pH 7.4, temperature 298 K, and 0.25 M salt, and the charges were assigned according to default settings using the "Compute | Protonate 3D" algorithm (Labute 2009) followed by energy minimization of the structure using the "Amber10:EHT" forcefield. Prior to docking, potential docking sites were identified on the protein by applying the "site finder" algorithm (Volkamer et al. 2010) to the selected atoms of the P450 polypeptide and the heme group. The algorithm returns binding sites on the protein, ranked according to size. For these simulations, the highest-ranked site (Site 1) was selected by the selection of placeholders known as "dummies" in the program. Ligands α–ES (**1a**), β–ES (**1b**), ES diol (**3**), ES lactone (**4**, both enantiomers), ES ether (**5**), and ES sulfate (**9**) were constructed in MOE using "builder" and a database of ligands was generated as a ".mdb" file.

Ligands were docked using all atoms of the polypeptide and the heme prosthetic group as the "receptor". Triangle matcher was the algorithm used for the placement of the ligands in the selected site. Ligand poses were scored by London dG and refined for an induced fit. Final scoring of poses utilized the GBVI/WSA dG (Generalized Born Volume Integral/ Weighted surface area) algorithm (Wojciechowski and Lesyng 2004, Labute 2008, Corbeil et al. 2012); a maximum of 30 poses were retained. The distribution of poses was estimated based on each structure's conformational energy. Conformational energy (E_{conf}) was obtained from the database with the retained poses and was in kcal/mol. The distribution of poses was estimated by assuming that all retained poses are in equilibrium and calculating a percentage of each pose based on the conformational energy. Distances between heme-iron and C2, C3, C5, C6 and C7 of the substrate, and angles at Fe to two carbon atoms in the substrate (*e.g.* C2-Fe-C7) were recorded and weighted according to the distribution of poses. Poses populated <10 % were not analyzed.

Results

Mutants obtained

The mutants obtained by SeSaM are listed in **Table 1**. In this ES-selected set of mutants, two mutations occurred twice: K314E and D297N. Furthermore, residue A296 was found to have mutated twice, but to different residues: A296V (in *ES*2) and A296P (in *ES*5). The selected variants had more than one mutation, except *ES*5 (A296P) and *ES*6 (G120S). Interestingly, mutation of K314 was also noticed in the set of mutants selected on 3-chloroindole we labeled *IND* (Kammoonah et al. 2018), and residue V247 was mutated to F in two cases (*ES*7 - Table 1 - and *IND*1 (Kammoonah et al. 2018)).

Table 1. Mutants of $P450_{cam}$ obtained by the selection of a SeSaM library on minimal media containing endosulfan (1) and *m*-CPBA

Mutant name	**Mutations**
*ES*1	T56A/N116H/D297N
*ES*2	F292S/A296V/K314E/P321T
*ES*3	Q108R/R290Q/I318N
*ES*4	S221R/I281N
*ES*5	A296P
*ES*6	G120S
*ES*7	V247F/D297N/K314E

Coupled assay optimization

The steady-state kinetic assay was optimized with crude *ES*7 lysate to obtain the conditions described in the methods. ES diol (**3**) and α-ES (**1a**) were compared at two concentrations, 100 μM and 200 μM, and in both cases, ES diol was the substrate that gave more product with absorbance at 506 nm (**Fig. 4 a** and **b**). To ensure that the product at 506 nm was not due to random activity, three controls were run alongside a dose-response with ES diol (**3**) and *ES*7 (**Fig. 4d**): 1) omitting the substrate but keeping the oxidative enzymes P450 and HRP, 2) omitting the P450 but using 500 μM of ES diol (**3**) and HRP and 3) omitting the HRP but using P450 and 500 μM of ES diol (**3**). This assay reveals a significant result: the formation of the colored 4-AAP adduct requires active P450 and the ES diol substrate, and it does not require HRP. When this 4-AAP assay is used in phenol analysis (Wong et al. 2005, Lülsdorf et al. 2015, Zeng et al. 2015), HRP is added to cause *in situ* formation of *ortho* or *para* quinones which then react with the 4-

AAP to give the adduct (**Fig. 3**). The observation that colored product formed in the absence of HRP suggests that the action of the P450 gives rise to a quinone. We decided to keep HRP in the assay mixture to ensure that other reagents, such as NADH, do not reduce the quinone formed by the action of the P450 on ES diol in the mixture. As seen in **Fig. 4** (c and d), the rate of formation of the colored product depended on the substrate concentration.

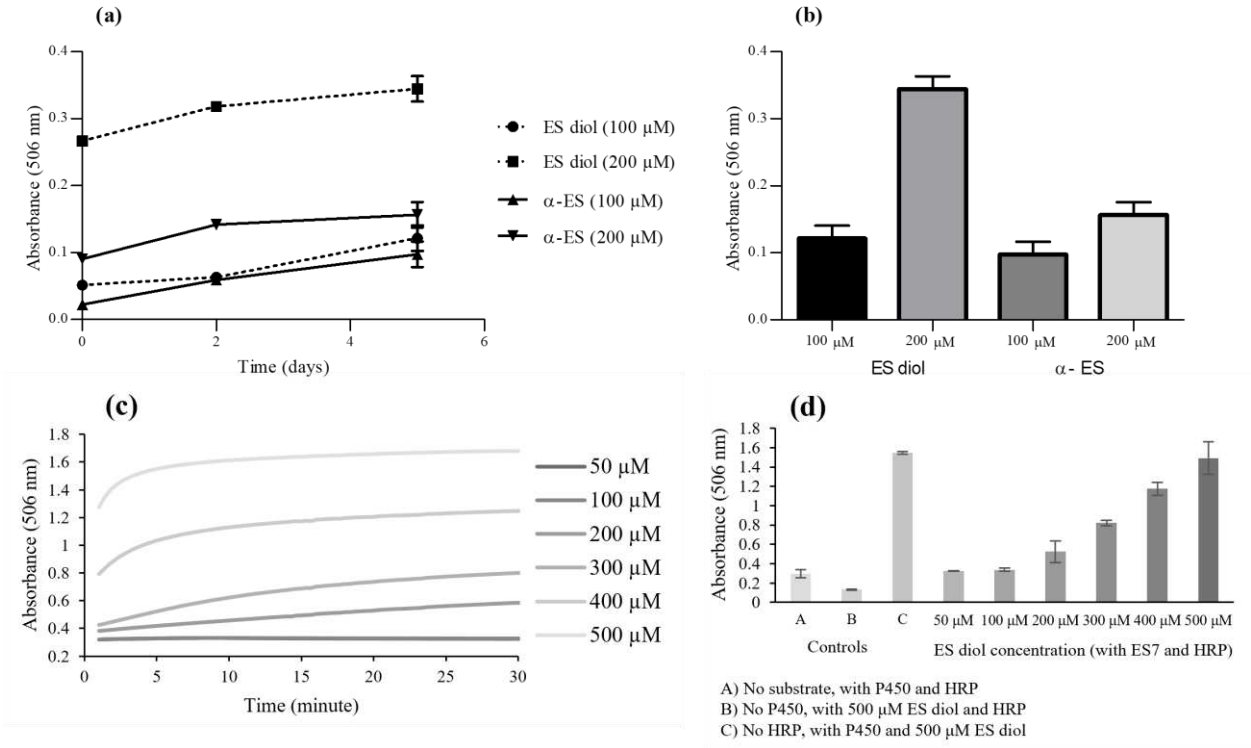

Fig. 4 *ES*7 and ES diol assay optimization (**a**) absorbance at 506 nm using ES diol and α-ES during a 5-day assay, (**b**) net absorbance at 506 nm using ES diol and α-ES after a 5-day assay, (**c**) total absorbance using different concentrations of ES diol (**3**) using *ES*7 in the coupled assay, (**d**) total absorbance at different concentration of ES diol (**3**) using *ES*7 coupled assay

Activity screen with crude lysates to find the most active mutant

The steady-state kinetic assays were performed using the crude lysates of WT-P450$_{cam}$ and mutants (*ES*1-*ES*7 and *IND*1), with ES diol (**3**) as a substrate. The metabolites were coupled with 4-AAP *in-situ* (as described above) and monitored at 506 nm (**Table 2** and **Fig. S10**). The *IND*1 mutant, selected previously for dechlorination of 3-chloroindole from the SeSaM library, was also included to compare its activity with the *ES* mutants because it had the highest 3-chloroindole dechlorination activity (Kammoonah et al. 2018). The rate of 4-AAP adduct formation was highest for the mutant *ES*2 in terms of turnover number (k_{cat}) and catalytic efficiency ($k_{cat}/K_{\mathbf{M}}$) followed by *ES*7. *ES*6, with a single mutation, was the least active of the *ES* mutants. WT-P450$_{cam}$ was significantly less active than the mutants (**Table 2**, **Fig. S10**). Despite being selected against 3-chloroindole, *IND*1 was one of the most active mutants for ES (**1**) turnover (**Table 2**). All these mutants followed sigmoidal kinetics, which required the use of an allosteric model (as opposed to the classic Michaelis Menten model) for analysis (**Fig. S10**).

Mutants *ES*2 and *ES*7 were chosen for further studies because of their comparatively high activity; mutants *ES*5 and *ES*6 were also chosen because they had a single mutation, yet showed higher activity than the WT. These P450$_{cam}$ mutants were prepared by site-directed mutagenesis using a recombinant wild type P450$_{cam}$ construct, with a cleavable histidine purification tag, as a template.

Table 2. Kinetic data of ES diol **3** with WT $P450_{cam}$ and mutants (using crude lysate)

Mutants	k_{cat} **(μM/s.μM P450)**	K_M **(μM)**	k_{cat}/K_M **(1/s.μM)**
WT [a]	0.8 ± 0.0	1024.6	0.8 ± 0.0 $\times 10^{-3}$
*IND*1 [b]	4.4 ± 0.5	363.3	12.0 ± 1.5 $\times 10^{-3}$
*ES*1	3.8 ± 1.1	393.2	9.6 ± 2.8 $\times 10^{-3}$
*ES*2	6.2 ± 2.3	372.8	16.6 ± 6.1 $\times 10^{-3}$
*ES*3	3.2 ± 0.2	443.8	7.2 ± 0.4 $\times 10^{-3}$
*ES*4	3.0 ± 0.6	318.6	9.3 ± 1.8 $\times 10^{-3}$
*ES*5	3.9 ± 1.1	371.3	10.4 ± 2.9 $\times 10^{-3}$
*ES*6	2.7 ± 0.5	387.8	7.0 ± 1.3 $\times 10^{-3}$
*ES*7	4.3 ± 1.2	332.3	12.8 ± 3.7 $\times 10^{-3}$

[a] WT data were estimated from the Lineweaver-Burk equation.

[b] *IND*1- E156G/V247F/V253G/F256S $P450_{cam}$

Recombinant $P450_{cam}$ mutants: stability and kinetics

The recombinant *ES*6 and *ES*7 $P450_{cam}$ mutants were successfully cloned, expressed, purified, and the His_6-tag was removed successfully from the P450 using Factor Xa. However, *ES*2, one of the most active mutants (**Table 2**), did not express well and could not be purified without the loss of heme. In addition, mutant *ES*5, which also had a mutation of A296 (like *ES*2), expressed well, but cleavage of the His_6-tag by Factor Xa protease resulted in secondary cleavage and undesired fragments (see **Fig. S11**), as well as heme loss. Thus, mutants *ES*2 and *ES*5 could not be produced by this method.

Due to the instability of mutant *ES*2, two variants of *ES*2 were generated: F292S/A296V and K314E. For these, F292S/A296V again did not express and lost the heme, whereas K314E did express (see below). Thus, we conclude that mutation of A296 is detrimental to the stability of $P450_{cam}$.

A recombinant clone of $P450_{cam}$ with K314E mutation was constructed, since both *ES*2 and *ES*7 share this mutation, to demonstrate the effect of K314E mutation on the stability and activity towards ES (**1**). Expression and purification of this variant were successful.

Steady-state kinetic assays were performed using purified WT and mutants *ES*6, *ES*7, and K314E, with ES diol (**3**) as a substrate. Increased catalytic activity (turnover number as well as catalytic efficiency) was noticed in the purified *ES*6 and *ES*7 mutants compared to the crude lysates used previously (2-fold and 2.5 fold respectively, **Table 2** and **Table 3**). Furthermore, the catalytic activity of *ES*7 was highest (~80-fold higher than WT), followed by *ES*6 and K314E (**Table 3**).

Table 3. Kinetic data of ES diol **3** with purified WT $P450_{cam}$ and mutants [a]

Mutant	**Mutations**	k_{cat} **(μM/s.μM P450)**	K_M **(μM)**	k_{cat}/K_M **(1/s.μM)**
WT [b]		0.15 ± 0.04	385	0.4 ± 0.1 $\times 10^{-3}$
*ES*2	F292S/A296V/ K314E/ P321T	n.d	n.d	n.d
*ES*5	A296P	n.d	n.d	n.d
F292S/ A296V	F292S/ A296V	n.d	n.d	n.d
K314E	K314E	3.8 ± 0.3	370	10.1 ± 0.7 $\times 10^{-3}$
*ES*6	G120S	5.7 ± 0.3	368	15.5 ± 0.9 $\times 10^{-3}$
*ES*7	V247F/D297N/ K314E	12.6 ± 4.7	394	31.9 ± 12.0 $\times 10^{-3}$
*ES*7 [c]	V247F/D297N/ K314E	1.4 ± 0.1	361	3.9 ± 0.1 $\times 10^{-3}$
*ES*7 [d]	V247F/D297N/ K314E	1.7 ± 0.2	28 ± 9	60.7 ± 0.7 $\times 10^{-3}$

[a] Plots of rate vs. substrate concentration of $P450_{cam}$ mutants are shown in **Fig. S12**.

[b] WT data were estimated from the Lineweaver-Burk equation

[c] *ES*7 mutant – using low concentration of *ES*7 with redox partners (**Fig. 5**)

[d] *ES*7 mutant – using *m*-CPBA as a shunt (**Fig. 6**)

n.d = Not determined because the mutant enzyme was unstable and could not be purified

In the experiments using crude lysate (**Table 2**) or purified proteins (**Table 3**), the reaction was robust, and we observed a rapid burst of product formation from endosulfan diol (**3**) degradation by $P450_{cam}$ mutants (**Fig. 4c**). It is important to note that full saturation of the rate could not be reached, because it was not possible to increase the substrate concentration due to the precipitation

above 500 μM. Thus, the values of k_{cat} and K_M shown in **Table 3** are best estimates, based on least-squares fitting of the data to an allosteric kinetic model (see methods) or to the Lineweaver-Burk equation for the WT. To verify the linearity of the initial rate of product formation, we performed experiments using a 2× lower concentration of the *ES*7 mutant (0.5 μM) and a higher concentration of PdX (6 μM) than before. We verified that the beginning of the progress curves was linear and still observed a sigmoidal pattern when plotting the initial velocity against substrate concentration. This indicates that the sigmoidal kinetics observed earlier and summarized in **Table 2** and **Table 3**, are not due to the concentration of $P450_{cam}$ or the ratio of $P450_{cam}$ to PdX (**Fig. 5**).

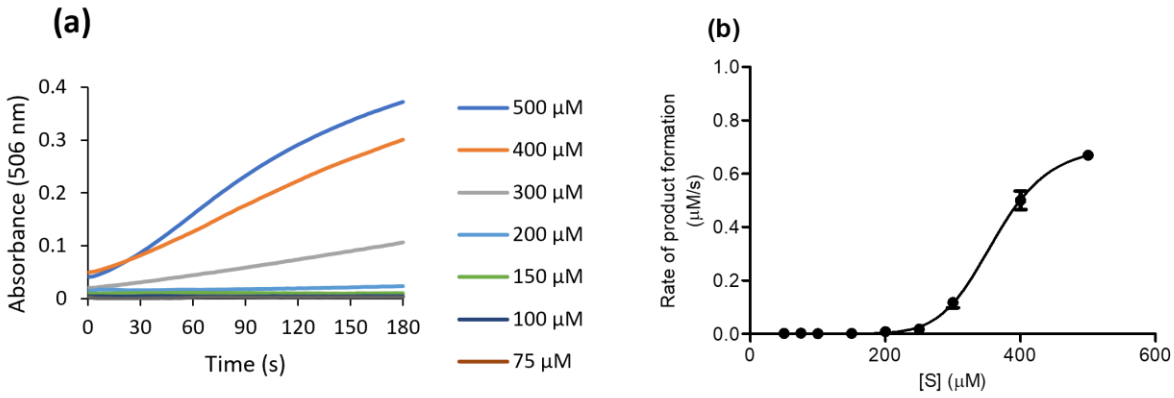

Fig. 5 Colorimetric assay of *ES*7 $P450_{cam}$ with redox partners (PdR, and PdX) and NADH with 4-AAP: (**a**) absorbance at 506 nm over time using different concentrations of ES diol (**3**), (**b**) steady-state kinetic assay of *ES*7 using ES diol (**3**). The rates are the best linear fits to the linear portion of the progress curves shown in (**a**)

Steady-state kinetic assay with the redox partners and NADH or *m*-CPBA (shunt pathway)

When mutant *ES*7 was shunted with *m*-CPBA, with ES diol (**3**) as substrate, it showed hyperbolic (Michaelis-Menten) kinetics. In contrast, when mutant *ES*7 was assayed with redox partners (PdX,

and PdR) and NADH, allosteric sigmoidal kinetics were observed with ES diol (**3**) as substrate (**Fig. 6**). Overall, the k_{cat} with *m*-CPBA was ~ 7× lower (1.7 ± 0.2 μM/s.μM P450) than with the redox partners (12.6 ± 4.7 μM/s.μM P450) (**Table 3**), but the K_M with *m*-CPBA was also lower than with the redox partners (**Table 3**).

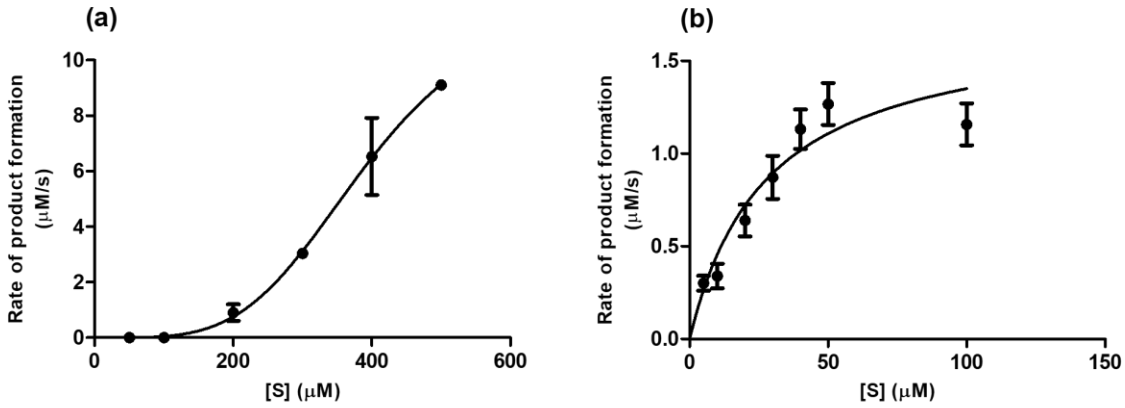

Fig. 6 Steady-state kinetic assays of *ES*7 using ES diol (**3**). (**a**) using redox partners (PdX and PdR) and NADH, and (**b**) using *m*-CPBA as a shunt

Assays with other hexachlorinated bicyclic substrates: substrate scope of *ES*6 and *ES*7

In order to compare the substrate scope between the active mutants *ES*6 and *ES*7 versus the WT $P450_{cam}$, kinetic assays were performed using various substrates (ES diol, ES sulfate, ES ether, ES α:β, ES lactone, and HC), in the same manner as for ES diol above (**Table 3**). These substrates gave sigmoidal kinetics and did not reach saturation (**Fig. S13**). To better compare the activities of WT, *ES*6, and *ES*7 against different substrates, assays were repeated at concentrations of 50 μM, 100 μM, and 200 μM. The rates of product formation for each enzyme at different substrate concentrations are shown in **Fig. 7**.

There was no significant difference between *ES*6 and *ES*7 ($p > 0.05$); however, WT $P450_{cam}$ was conspicuously less active than both mutants. More specifically, at 50 μM substrate concentration, the WT enzyme showed no detectable activity with any substrate, whereas the mutants showed activity, with the highest being for ES α:β (**1**) and HC (**2**). Activities with ES diol (**3**) and ES lactone (**4**) were undetectable. Significant differences between WT and mutants ($p < 0.05$) were noticed with ES ether (**5**), ES sulfate (**9**), ES α:β (**1**), and HC (**2**). The WT had no detectable activity at 100 μM substrate concentration, but the mutants did. *ES*6 and *ES*7 were more active with ES ether (**5**) and HC (**2**) than with other substrates. The least activity was noticed with ES diol (**3**), while once again, no activity was detected with ES lactone (**4**). Significant differences between mutants and WT ($p < 0.05$) were noticed with ES diol (**3**), ES ether (**5**), ES sulfate (**9**), ES α:β (**1**), and HC (**2**). Lastly, at 200 μM substrate concentration, some activity was evident for the WT, but it was still much lower than the mutants. The highest activity was noticed with ES ether (**5**) for every enzyme. The mutants were also quite active with HC and least active with ES diol. This time, there was some activity with ES lactone (**4**) that was interestingly higher than with ES diol (**3**). Significant differences between WT and mutants ($p < 0.05$) were noticed with ES diol (**3**), ES ether (**5**), ES sulfate (**9**), and ES α:β (**1**). Interestingly, HC (**2**) and ES lactone (**4**) did not differ significantly between the mutants and WT ($p > 0.05$), which suggests that WT can turn some of these compounds over but at a very high substrate concentration.

Overall, ES ether (**5**) was the substrate best turned over by *ES*6 and *ES*7, followed by HC (**2**). Both mutants showed intermediate activity against ES α:β (**1**), the substrate originally used to select the mutants, and ES sulfate (**9**). The least activity was noticed against ES diol (**3**) and ES lactone (**4**). At the lowest substrate concentrations of 50 μM and 100 μM, the WT $P450_{cam}$ showed

no detectable activity, and at 200 µM, it showed some activity, but this was approximately three times less than the mutants.

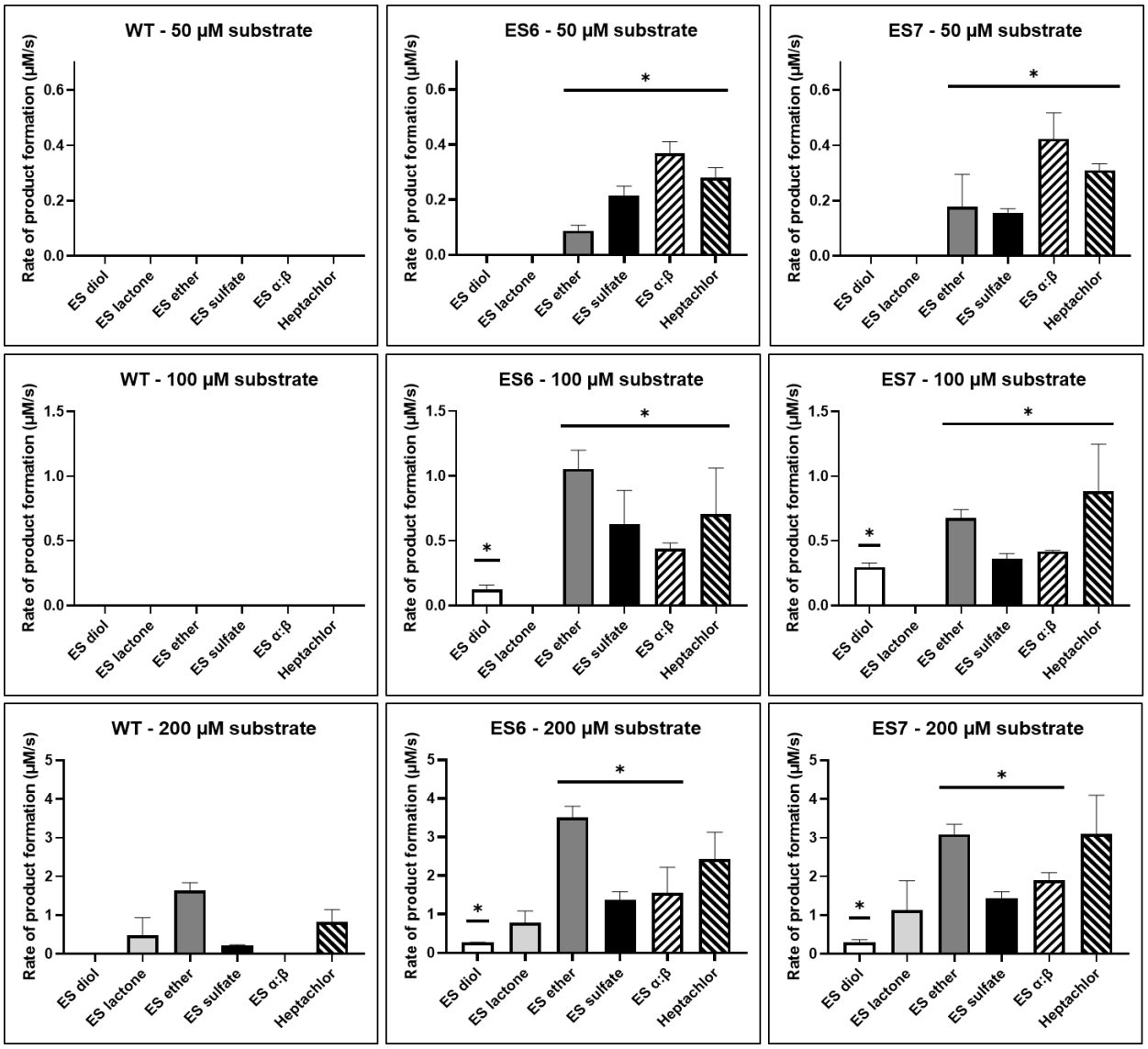

Fig. 7 Kinetic comparison of WT-P450$_{cam}$ and mutants *ES*6 and *ES*7 with various substrates (ES diol, ES lactone, ES α:β, ES ether, ES sulfate, and HC) at concentrations of 50 µM, 100 µM, 200 µM. Bars represent means ± S. E. of three replicates. The * denotes a significant difference in activity relative to the WT (Student t-test, $p < 0.05$)

Ligand binding and dissociation constant (K_d) using selected purified mutants and WT-P450$_{cam}$

Dissociation constants (K_d) were measured using the change in spin shift of the P450, often seen upon substrate binding. WT-P450$_{cam}$ shows a characteristic peak (λ_{max} 418 nm – low spin Fe-III) without camphor (natural substrate) and on the addition of camphor, this peak is blue-shifted (λ_{max} 392 nm – high spin Fe-III) due to the change in the spin state of iron (Fe) in the heme molecule (**Fig. 8**) (Atkins and Sligar 1988, Schulze et al. 1996). On titrating mutants and WT-P450$_{cam}$ with ES diol (**3**), the spin change of Fe in heme was observed (**Fig. 8**). As the substrate is titrated into the enzyme, this change in spin state is used to calculate K_d values for ES diol (**Table 4**). Using camphor as substrate, K_d for WT-P450$_{cam}$ was found 1.7 ± 0.04 μM (1.6 ± 0.3 μM (Atkins and Sligar 1988)). K314E mutant binds camphor more strongly than WT with K_d value 1.0 ± 0.04 μM. However, *ES*6 and *ES*7 showed higher K_d values for camphor and ES diol than WT-P450$_{cam}$ (**Table 4**). Similar patterns of K_d values for WT-P450$_{cam}$ and mutants were observed with ES diol (**Table 4**). However, overall K_d values of ES diol were 13-45 × higher than those for camphor, indicating that these enzymes had a lower affinity for ES diol than for camphor. Interestingly, with camphor, the binding isotherms fit a one-site binding model very well, but for ES diol, the isotherms were not completely hyperbolic. This phenomenon can be seen with WT and *ES*7 (**Fig. 8)** and with *ES*6 and K314E (**Fig. S14**).

Table 4. Dissociation constant measured using camphor and ES diol **3** with purified WT $P450_{cam}$ and mutants

Mutants	**Mutations**	**(1*R*)-(+)-Camphor K_d (μM)**	**ES diol (3) K_d (μM)**
WT	-	1.7 ± 0.04	41.6 ± 5.5
K314E	K314E	1.0 ± 0.04	31.3 ± 3.7
*ES*6	G120S	2.4 ± 0.05	108.9 ± 27.4
*ES*7	V247F/D297N/K314E	10.4 ± 0.43	143.2 ± 17.4

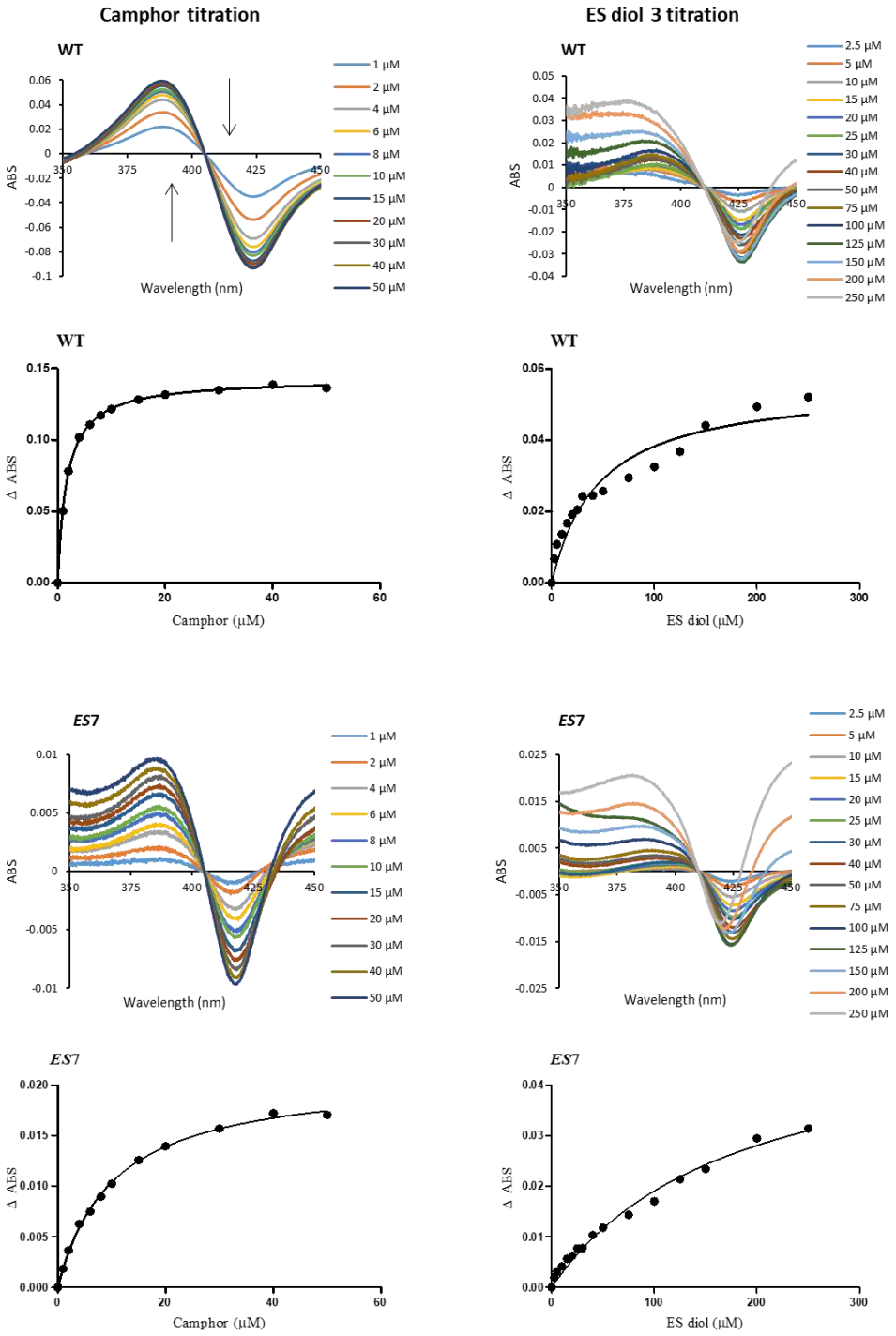

Fig. 8 Titrations of wild type (WT) $P450_{cam}$ (top) and mutant *ES*7 (bottom) with camphor (left set of graphs) or ES diol (**3**) (right set of graphs). The spectra (top set of graphs for each enzyme) show the blue shift in the Soret band as the substrate is titrated into the enzyme preparation. The

isotherms (lower set of graphs for each enzyme) depict the change in the Soret band (the increase in absorption at the blue-shifted wavelength relative to the decrease in absorption of the original Soret band)

Chloride release with purified WT-P450$_{cam}$ and *ES*7

Using the *ES*7 mutant, chloride ions released were detected instantly upon adding ES diol (**3**) (300 and 500 μM) to the reaction mixture. However, NADH was found to enhance chloride electrode readings and give overestimates, whereas NAD^+ was found to suppress chloride readings, giving underestimates (**Fig. S15**). Alcohol dehydrogenase was used to regenerate NADH *in situ*, to maintain a constant level of NADH. However, a slower rate of NADH production by alcohol dehydrogenase (1 nmol/minute) than NADH being used by *ES*7-P450$_{cam}$ mutant resulted in lower chloride ion readings than expected (**Fig. S16**). For this reason, chloride release experiments were repeated without the redox partner system and NADH, using only the purified P450 enzyme and *m*-CPBA as a shunting agent (**Fig. S17**). Overall, chloride release was detected with the *ES*7 mutant, while with WT-P450$_{cam}$ (ES diol 500 μM), chloride ion release was not detected (**Fig. 9**). Colorimetric analysis of product formation from chloride release assays revealed that, on average, 5.2 ± 0.7 and 5.7 ± 0.2 chloride ions were released per colored product formed by the *ES*7 mutant using non-labeled ES diol (**3**) and ^{13}C-ES diol, respectively (**Table 5**).

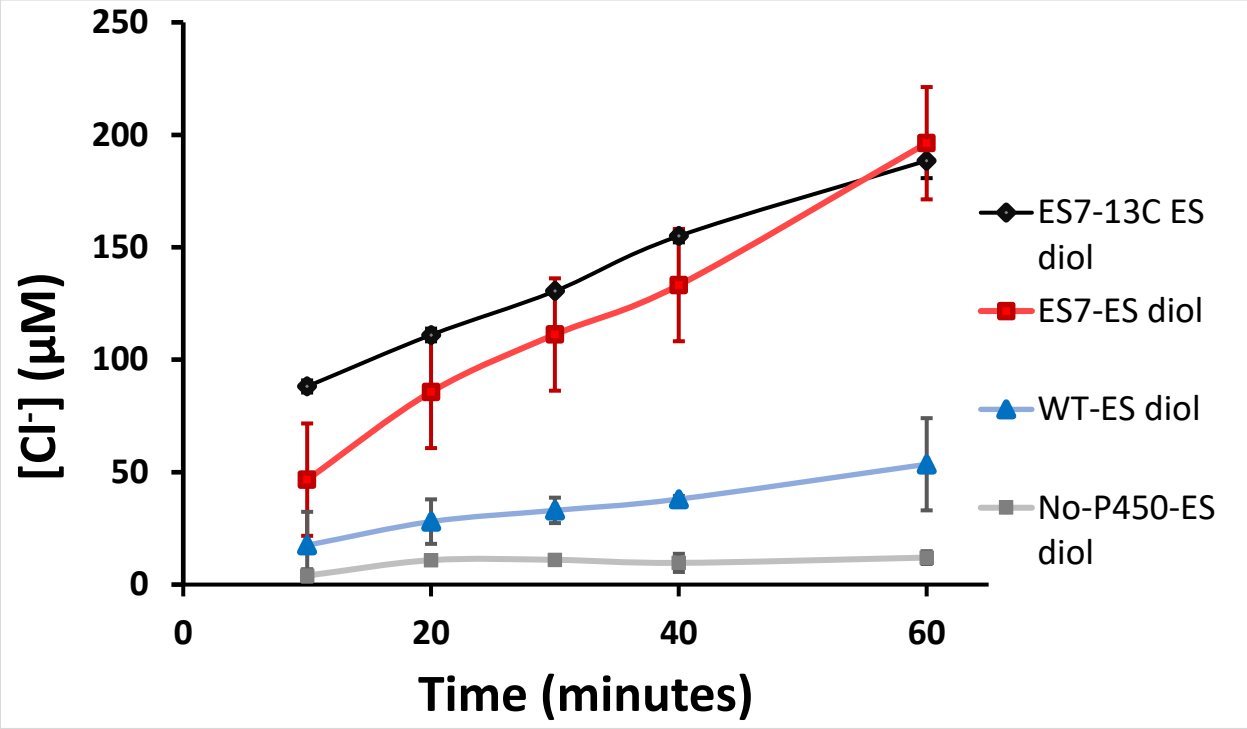

Fig. 9 Chloride release using ES diol (**3**) and *m*-CPBA**,** with WT-P450$_{cam}$ (ES diol **3** 300 µM), *ES*7 (^{13}C-ES diol **3** 300 µM), *ES*7 (ES diol **3** 300 µM) and No P450$_{cam}$ control. Points represent the mean ± standard deviation of 3 replicates

Table 5. The ratio of chloride ions released to quinone (4-AAP coupled) formed in assay with *m*-CPBA as shunting agent

Conditions	**Chloride [Cl-] ions detected (µM)[a]**	**4-AAP coupled-product (µM)[a]**	**Ratio (Cl^- per quinone)[a]**
*ES*7, ES diol (3), and *m*-CPBA	196 ± 32	38 ± 5	5.2 ± 0.7
*ES*7, ^{13}C-ES diol, and *m*-CPBA	188 ± 8	35 ± 6	5.7 ± 0.2
WT ES diol (3), and *m*-CPBA	53 ± 20	23 ± 6	2.3 ± 0.6
ES diol (3) and *m*-CPBA only (control)	12 ± 3	0	0

[a] Values are the mean ± standard deviation of 3 replicates.

Products formed in experiments with ES diol

The mixture of coupled products formed in colorimetric experiments was analyzed by LC-MS, and the adduct between 4,5-dihydroxyphthalide **16** and 4-AAP was detected by matching retention time and mass spectrum (**Fig. S18**).

The product formed during the chloride release experiment was 1,2-dihydroxy-4-hydroxymethylbenzene (or 4-hydroxymethylcatechol), as determined by ^{13}C-NMR against a commercial standard of veratryl alcohol (1,2-dimethoxy-4-hydroxymethylbenzene) (**Fig. S19**).

Experiment with ES lactone and product detection by GC-MS

The dehalogenation of ES lactone gave rise to 4,5-dihydroxyphthalide (**16**) which was converted to 4,5-dimethoxyphthalide (**15**) by reaction with BF_3/MeOH. The product peak matched exactly

the retention time and spectrum of standard **15** (**Fig. 10**). The product detected formed at a specific rate of of ~ 20 ± 9 pmol min^{-1} nmol $P450^{-1}$ (three replicates), which is in the same order of magnitude as the specific rate observed colorimetrically in **Fig. 7** (~ 36 pmol min^{-1} nmol $P450^{-1}$). In the overnight incubation we also observed traces of reduced products (wherein one phenol was lost – two isomers – or both phenol OH groups had been lost, phthalide).

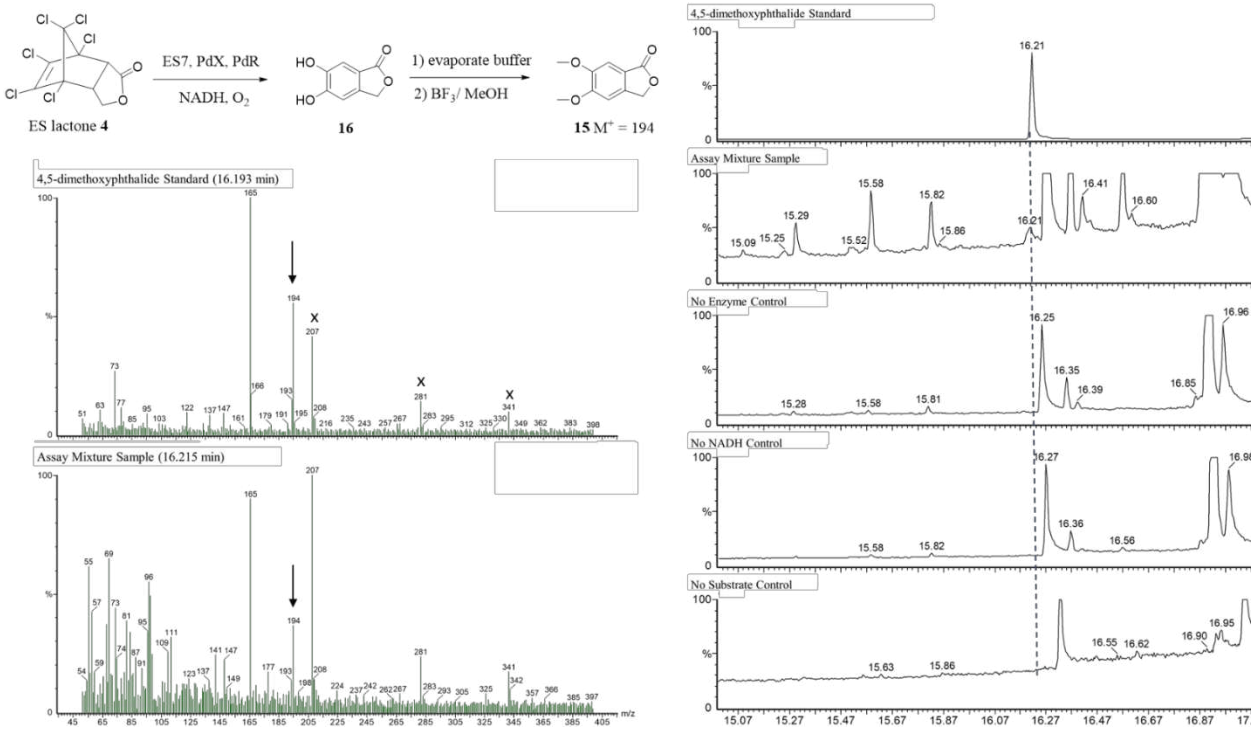

Fig. 10 Dehalogenation of ES lactone with P450 *ES*7, derivatization of the product by BF_3/MeOH and analysis by GC-MS. Compound **15** (4,5-dimethoxyphthalide) was detected at 16.2 min in the enzymatic reaction isolates and was absent from the controls. The spectrum of the product matched the spectrum of synthetic compound **15** (M+ 194). Ions at m/z 207, 281 and 341 are part of the background

***In-silico* docking studies**

Analysis of docked substrates, such as ES diol, revealed that the WT and active mutants differed by the relative orientation of the double bond and the heme iron. In the WT, the most populated pose of ES diol (**3**) had the iron in the same plane as the double bond, whereas the most active mutants (*ES*7 and *ES*2) had the iron poised above the double bond, on the same side as the bridge (**Fig. 11**). The pose in the WT is not suitable for oxidation because the π-bond in the substrate needs to be oxidized by the iron-oxo moiety of the P450 to initiate the dehalogenation cascade proposed below. We used the angle C2-Fe-C7 to measure how the substrate was tilted above the iron in the most populated pose obtained in the modeling studies. Thus, ES diol in the WT had a much smaller angle than ES diol in the most active mutants. There was a positive correlation between the C2-Fe-C7 angle and the activity we observed with the crude enzymes (**Table 2**), suggesting that the positioning of the double bond above the iron is essential for activity.

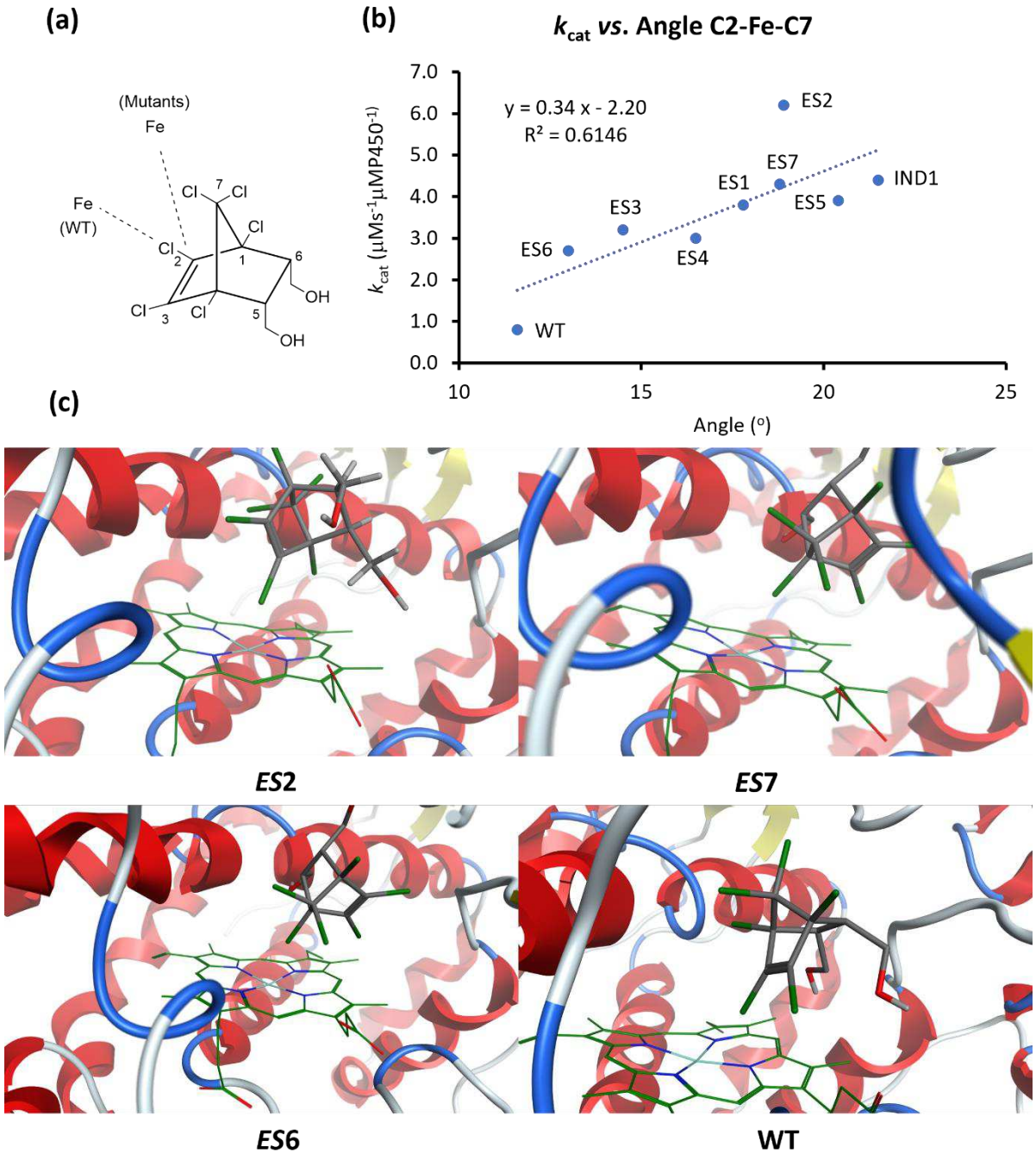

Fig. 11 Analysis of ES diol (**3**) positioning in the $P450_{cam}$ active site by *in silico* docking. (**a**) Numbering of carbons in ES diol. The dashed lines to Fe show the different positions of Fe relative to the C2=C3 double bond we found: in the plane of the double bond, with one Cl atom pointing at Fe, for WT, and above the plane on the side of the bridge for the most active mutants. (**b**) Plot

of k_{cat} found for the various mutants with crude extracts (data in **Table 2**) vs. the angle C2-Fe-C7 for the most populated pose in each mutant. (**c**) Views of the most populated pose of ES diol (**3**) in the active sites of *ES*2, *ES*7, *ES*6, and WT

Discussion

Proposed mechanism of dehalogenation

Previously reported dehalogenation studies of chlorinated organic compounds by WT-$P450_{cam}$ were limited to small organochlorine compounds, including halomethanes, tri-, tetra, penta-, and hexa-chloroethane, tetrachloroethene, and dichloropropane. These studies were done under low oxygen conditions resulting in reductive dehalogenation of those substrates (Li and Wackett 1993, Logan et al. 1993, Lefever and Wackett 1994, Wackett et al. 1994, Wackett 1995). Studies done with vinylidine chloride and microsomal liver P450s were done under oxidizing conditions (Liebler and Guengerich 1983). In this study, dehalogenation of endosulfan diol was investigated using $P450_{cam}$ mutants under oxidizing conditions. We detected aromatic products **16**, **20**, **21** and **22**. We demonstrated that they come from ES diol and that their formation is coupled with the loss of ~ 6 chloride ions on average. Based on these observations, we propose a mechanism for the dehalogenation of endosulfan diol by these mutants (**Fig. 12**).

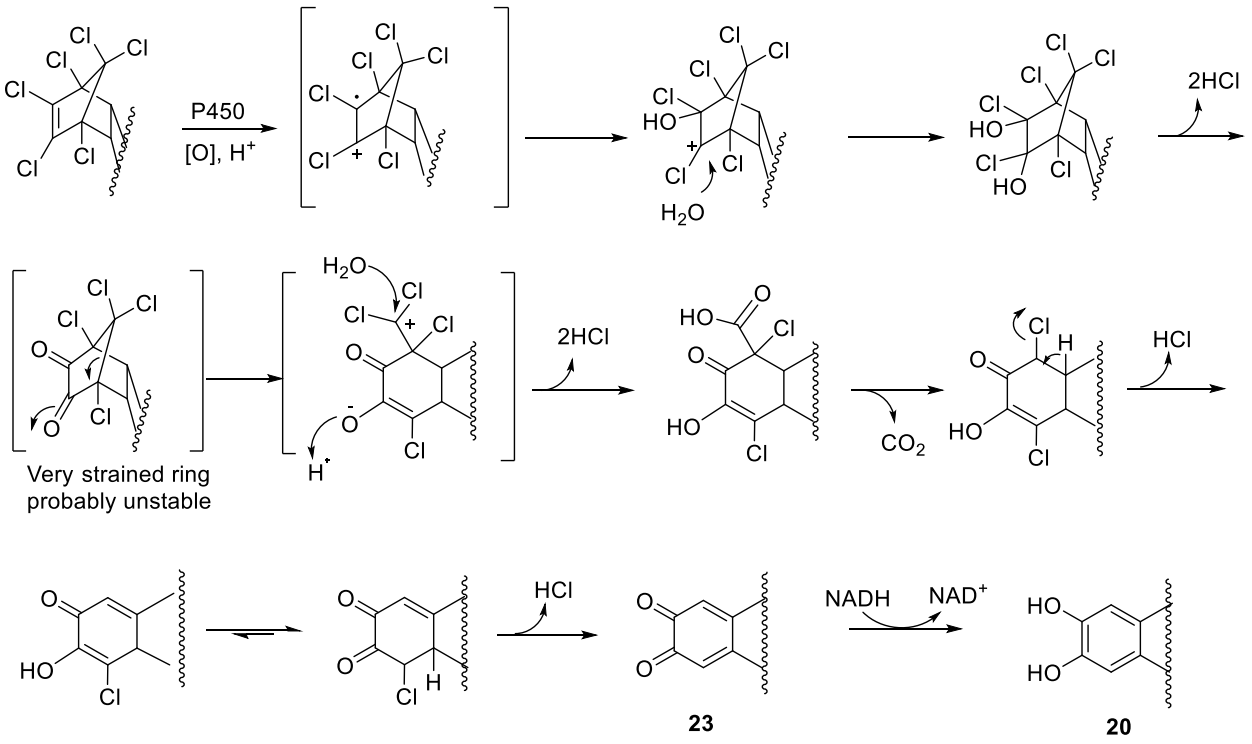

Fig. 12 Proposed mechanism of degradation of the bicyclic core of ES and related substrates by $P450_{cam}$ mutants, such as *ES*7. The proposed route accounts for the loss of 6 Cl^- ions from the ES diol core structure and of the bridge as CO_2

The proposed mechanism of dehalogenation starts with 1-electron oxidation of the sterically hindered and electron-poor double bond of the ES system by the P450. This results in a radical cation and Compound II (**Fig. S20**). The protonated form of Compound II has an estimated pK_a of 8.2 in chloroperoxidase (Green et al. 2004), and it should be similar in $P450_{cam}$, thus, it should be protonated at the pH of our assay (7.4). The radical cation can be trapped by the OH radical on the iron (the rebound mechanism – transfer of OH radical from protonated Compound II) and a water molecule, respectively (**Fig. S20**). This leads to two geminal chlorohydrin moieties that lose HCl to give the vicinal diketone. This intermediate is likely very unstable due to bond angle strain, which is relieved by opening of the bridge. Hydrolysis of the geminal dichloromethyl cation from

the bridge gives a carboxylic acid group, which can decarboxylate because it is β to a ketone. Two rounds of HCl elimination from the appropriate tautomers lead to *o*-quinone **23**, which can be reduced non-enzymatically by the NADH present in the mixture (see below). Consistent with the initial formation of an *o*-quinone, we observed a colored product in the 4-AAP coupled assay in the absence of HRP and H_2O_2 (**Fig. 4d**).

One alternative to the addition of an OH radical from protonated Compound II to the radical cation, resulting from initial one-electron oxidation of the substrate, is the addition of the oxygen of Compound II to the carbon radical (**Fig. S20**). This is the same type of intermediate proposed by Liebler and Guengerich (1983) for the oxidation of vinylidene chloride. Elimination of chloride from this intermediate would then result in a keto moiety. Meanwhile, addition of water to the cation would result in the chlorohydrin, which then eliminates HCl to furnish the second keto group of the strained intermediate.

In either case, we believe that an epoxide is not involved in the early step of this reaction, because of the following observations: 1) when ES congeners were incubated in buffer with *m*-CPBA without the enzyme, no product formed and 2) ES congeners did not react with *m*-CPBA in chloroform. The double bond of ES congeners is too electron poor and sterically hindered to form an epoxide.

This oxidative dehalogenation of ES diol was observed under two conditions: 1) using the redox partners of $P450_{cam}$, PdR, and PdX and the natural electron donor NADH and O_2 from the air, or 2) using an artificial shunting agent, *m*-CPBA, with the $P450_{cam}$ mutants. Both conditions are oxidizing, whereas previously observed dehalogenation of polychlorinated ethane congeners by $P450_{cam}$ was proposed to involve a two-electron reduction of the substrate under low oxygen conditions (Li and Wackett 1993). A study with vinylidene chloride, in which hepatic P450s

converted this compound to 2-chloro acetic acid or 2,2-dichloroacetaldehyde, resembles our study in that the double bond of the substrate was oxidized initially by a 1-electron oxidation, followed by addition of oxygen to one side of the double bond and collapse of that intermediate to the final products. These authors also showed that an epoxide was not the competent intermediate for the observed enzyme-catalyzed reaction (Liebler and Guengerich 1983).

Consistent with the proposed dehalogenation, the release of chloride ions was detected and quantified using a chloride ion electrode, and we have found close to 6 chloride ions released per quinone product formed, as would be expected for the proposed mechanism. To our knowledge, this is the first report of the biodegradation of ES and HC that involves removal of the chlorine atoms from the bicyclic core.

Reduction of o-quinones fromed in the dehalogenation reaction

Quinone **23** is reduced to the corresponding catechol, so when we isolated products, we obtained catechols or even further reduced products wherein catechol hydroxyl groups were removed (see below). *Ortho* quinones have been shown to be reduced non-enzymatically to catechol by NADH (Hirakawa et al. 2002). When we performed the reaction in the absence of NADH, using *m*-CPBA as a shunting agent for the P450, we also detected catechols. In these cases, the *o*-quinone formed could have been reduced by the electrode (in the chloride release measurement assays) or by peroxo radicals, which would form under those conditions. It has been shown that, e.g., *o*-quinones in polydopamine can be reduced by hydroperoxo radicals to the corresponding semiquinones and further to the catechols (Guo et al. 2021).

In a preliminary study, in which we transformed *ES*7 into *P. putida* (ATCC17453) and incubated that with ES (**1**), phthaldialdehyde was isolated from the culture mixture after a few days of

incubation, which suggests that two processes happened, in addition to the dechlorination: 1) hydrolysis and oxidation of ES to the corresponding dialdehyde and 2) reduction of the *o*-quinone, first to phenols and then to the benzene moiety (Prasad 2013). Because the initially formed *o*-quinone can be reduced to phenols, HRP and H_2O_2 were added in our assays to convert phenolic metabolites back to quinones and quantify them as 4-AAP adducts.

In the experiment with ES lactone and diol, we also observed reduced products, in which the catechol OH groups are removed after its formation. This can occur if there is tautomerism of the phenol to the corresponding cyclohexadienone, reduction of the keto group and elimination of water from the resulting secondary alcohol (**Fig. S21**).

Previously reported degradation of ES and heptachlor congeners

Previously reported biodegradation of endosulfan by fungal strains (*Phanerochaete chrysosporiu* (Kullman and Matsumura 1996), *Aspergillus terreus* and *Cladosporium oxysporum* (Mukherjee and Mittal 2005), *Mortierella* sp. (Kataoka et al. 2010), *Chaetosartorya stromatoides* and *Aspergillus terricola* (Hussain et al. 2007)) or bacterial strains (*Pseudomonas spinosa*, *Pseudomonas aeruginosa*, and *Burkholderia cepacian* (Hussainet al. 2007), *Mycobacterium* sp. (Sutherland et al. 2002), *Pandoraea* sp. , (Siddique et al. 2003) and *Klebsiella pneumoniae* (Kwon et al. 2002)), to list a few, resulted in endosulfan metabolites with the hexachlorinated bicyclic framework intact, such as ES diol (**Fig. 2**), but did not produce any dechlorinated products. We have shown here that *ES*6 and *ES*7 can dechlorinate several ES metabolites, such as the sulfate, ether, diol or lactone, found in earlier studies.

Heptachlor has the same hexachlorinated bicyclic core structure as ES, and we demonstrated that mutants *ES*6 and *ES*7 can turn HC over as well, giving colored quinone adducts in the assay.

This is only possible if the bicyclic core is dechlorinated, as proposed for the ES family of compounds. The earliest studies on heptachlor degradation include conversion to heptachlor epoxide in animals, plants (Gannon and Decker 1958) and soil (Gannon and Bigger 1958). Hydrolysis, epoxidation, and reduction of heptachlor are usually observed through soil microorganisms such as fungi, bacteria, and actinomycetes (Miles et al. 1969). Recent studies found microbial strains that metabolize heptachlor and its recalcitrant metabolite heptachlor epoxide. White rot fungi of the genus *Phlebia* degrade both heptachlor and heptachlor epoxide (Xiao et al. 2011) while *Pleurotus ostreatus* can also bioremediate contaminated soil (Purnomo et al. 2014). The soil bacteria *Bacillus cereus, Bacillus subtilis* and *Pseudomonas putida* have been found to degrade these compounds too. Other bacteria that have been reported to slowly degrade HC in soil include the novel 'strain H', which is similar to the genus *Shigella* or *Escherichia* (Qiu et al. 2018), *Pseudomonas fluorescens* or a blend of *Pseudomonas fluorescens, Bacillus polymyxa, Micrococcus flavus,* and *Flavobacterium* sp. (Doolotkeldieva et al. 2021) In all these studies, in which disappearance of HC is monitored, it is not clear whether the hexachlorinated bicyclic nucleus of HC is dehalogenated.

Mutation of $P450_{cam}$ to accommodate the new ES and HC substrates

In our study, wild-type $P450_{cam}$ did not show significant dehalogenation activity. In contrast, the mutants previously selected on minimal media with endosulfan and *m*-CPBA (Kammoonah et al. 2018) were significantly more active in the dechlorination of ES and HC substrates than the wild type. Cytochrome $P450_{cam}$ is known for its regio- and stereoselective oxidation of camphor to 5-*exo*-hydroxycamphor (Prasad et al. 2011). The ES and HC substrates are larger than camphor, though their bicyclic core resembles it.

To accommodate substrates with different size and/or shape than camphor, several amino acid residues in the catalytic site of $P450_{cam}$ have been mutated rationally (Bell et al. 2003, Denisov et al. 2005, Cook et al. 2016). Leu 244, Val 247, and Val 295, which make hydrophobic contacts with camphor bound in the active site (Poulos, Finzel et al. 1985), have also been mutated to study the oxidation of different hydrophobic substrates. In our case, V247 and D297, which were mutated in *ES*7 (V247F/D297N/K314E), are the only residues that were reported to have been mutated in the literature. Val 247 was previously mutated along with F87, Y96, and other actie site residues to study terpene oxidation (V247L) (Bell et al. 2003), propane and butane oxidation (V247L) (Bell et al. 2003), hexane oxidation (V247A/L), and benzylic oxidation of ethylbenzene (V247L/M/A) (Loida and Sligar 1993, Eichler et al. 2016). However, D297 residue was mutated previously only to study propane and butane oxidation (D297M) (Bell et al. 2003). The other residues (T56, Q108, N116, G120, S221, I281, R290, F292, A296, K314, I318, and P321) we found in our set of mutants have never been reported to have been altered.

Residue K314, which was mutated in two cases of the *ES* series and one of the *IND* series has been found to play an important role in conformational dynamics and PdX-mediated allostery in $P450_{cam}$ (Skinner et al. 2021). The binding of PdX to $P450_{cam}$ induces displacement in helix C, which is then transmitted to helix B′ and other helices (B, E, F, G, and I) on the distal end of the $P450_{cam}$ (Pochapsky et al. 2003, Myers, Lee et al. 2013, Tripathi et al. 2013, Pochapsky and Pochapsky 2019). Displacements in helices F and G are the main features of the transition from the open (substrate-free) to the closed (substrate-bound) forms, while helix B' is present near the active site of $P450_{cam}$ (Lee et al. 2010). Different spectroscopic data show that PdX favors the open-conformation of $P450_{cam}$ (or causes the P450 to change from the closed state to the open state) (Unno et al. 1997, Hiruma, Hass et al. 2013, Tripathi et al. 2013, Pochapsky and Pochapsky

2019). It is suggested that the reduced PdX transfers the electrons to a substrate-bound closed conformation of $P450_{cam}$, giving the ferric-hydroperoxo complex bound to oxidized PdX. The oxidized PdX is proposed to convert this back into the open conformation (Myers, Lee et al. 2013). In our selected $P450_{cam}$ mutants, some of the mutations are located in these helices, showing some displacement upon PdX binding. For example, Q108R (*ES*3), N116H (*ES*1), and G120S (*ES*6) mutations are located on helix C directly at the binding site of PdX. These mutations may play a similar effector role as PdX or enhance it in the presence of PdX. Mutation S221R in helix H can induce displacement in the F/G helices to affect the dynamics between the open and closed conformations of $P450_{cam}$.

In our ES diol (**3**) degradation studies using $P450_{cam}$ mutants with PdX and PdR to route the electrons from NADH, we observed allosteric sigmoidal kinetics (**Fig. S11**). These sigmoidal patterns of kinetics indicate that, due to the higher dissociation constant (K_d) of ES diol (**3**) compared to camphor (**Table 4**), we need a higher concentration of ES diol (**3**) to fully saturate the P450s in the closed conformation, to notice the catalytic activity with PdX and PdR than in their absence. The sigmoidal kinetics observed in the presence of PdX and PdR, are likely due to a rate-limiting step between substrate binding and the formation of Cpd I, which probably requires a closed conformation of P450s. Cpd I is needed to oxidize the electron-poor double bond of ES diol (**3**), as we have proposed. Consistent with this interpretation, we observed hyperbolic kinetics when we used *m*-CPBA as shunt which allows the enzyme to access Cpd I directly (**Fig. 6**).

Conclusion

We have found mutants of $P450_{cam}$ that oxidize the double bond of ES and related substrates, such as ES diol, sulfate, ether, and lactone, as well as heptachlor, such that the hexachlorinated

bicyclic system eliminates chloride and forms quinones. We propose a mechanism for this dehalogenation process, where six HCl molecules are released per molecule of ES diol after the double bond has been oxidized, consistent with our various experimental observations. To our knowledge, this is the first report of a cytochrome P450 capable of dehalogenating compounds such as ES or HC under oxidizing conditions.

Acknowledgements

This research was funded by a Natural Sciences and Engineering Research Council of Canada (NSERC) Discovery Grant (06088) and Discovery Accelerator Supplement (477793) to E.P. We thank Simon Fraser University for graduate fellowship support to A. R. and N. G.

Accession Codes

The sequences of the $P450_{cam}$ system include:

$P450_{cam}$ (Cam C) UniProt M5B4L7

PdX (Cam B) UniProt P00259

PdR (Cam A) UniProt P16640

The structure we used for modelling (reference 44) has PDB entry 2L8M

References

Armarego, W. L. F. and D. D. Perrin (1997) Purification of Laboratory Chemicals. Bath, UK, Butterworth Heinemann.

Asciutto, E. K., M. Dang, S. S. Pochapsky, J. D. Madura and T. C. Pochapsky (2011) Experimentally Restrained Molecular Dynamics Simulations for Characterizing the Open States of Cytochrome $P450_{cam}$. Biochemistry 50: 1664-1671.

Atkins, W. M. and S. G. Sligar (1988) The Roles of Active Site Hydrogen Bonding in Cytochrome P-450cam as Revealed by Site-Directed Mutagenesis. J. Biol. Chem. 263: 18842-18849.

Auclair, K., P. Moënne-Loccoz and P. R. Ortiz de Montellano (2001) Roles of the Proximal Heme Thiolate Ligand in Cytochrome $P450_{cam}$. J. Am. Chem. Soc. 123: 4877-4885.

Bell, S., X. Chen, R. J. Sowden, F. Xu, J. N. Williams, L. L. Wong and Z. Rao (2003). Molecular Recognition in (+)-α-Pinene Oxidation by Cytochrome P450cam. J. Am. Chem. Soc. 125: 705-714.

Bell, S. G., E. Orton, H. Boyd, J. A. Stevenson, A. Riddle, S. Campbell and L. L. Wong (2003). Engineering Cytochrome $P450_{cam}$ into an Alkane Hydroxylase. Dalton Trans. 11: 2133-2140.

Cook, D. J., J. D. Finnigan, K. Cook, G. W. Black and S. J. Charnock (2016). Cytochromes P450: History, Classes, Catalytic Mechanism, and Industrial Application. Advances in Protein Chemistry and Structural Biology. C. Z. Christov, Academic Press. 105.

Corbeil, C. R., C. I. Williams and P. Labute (2012). Variability in docking success rates due to dataset preparation. Journal of Computer-Aided Molecular Design 26(6): 775-786.

Cryle, M. J. and J. J. D. Voss (2006). Is the Ferric Hydroperoxy Species Responsible for Sulfur Oxidation in Cytochrome P450s? Angew. Chem. Int. Ed. 45: 8221-8223.

Dawson, A. H., M. Eddleston, L. Senarathna, F. Mohamed, I. Gawarammana, S. J. Bowe, G. Manuweera and N. A. Buckley (2010). Acute human lethal toxicity of agricultural pesticides: a prospective cohort study. PLoS Med 7(10): e1000357.

Denisov, I. G., T. M. Makris, S. G. Sligar and I. Schlichting (2005). Structure and Chemistry of Cytochrome P450. Chem. Rev. 105: 2253-2278.

Doolotkeldieva, T., S. Bobusheva and M. Konurbaeva (2021). The Improving Conditions for the Aerobic Bacteria Performing the Degradation of Obsolete Pesticides in Polluted Soils. Air Soil Water Res 14: 1-14.

Eichler, A., L. Gricman, S. Herter, P. P. Kelly, N. J. Turner, J. Pleiss and S. L. Flitsch (2016). Enantioselective Benzylic Hydroxylation Catalysed by P450 Monooxygenases: Characterisation of a P450cam Mutant Library and Molecular Modelling. Chembiochem 17(5): 426-432.

Enhui, Z., C. Na, L. MengYun, L. Jia, L. Dan, Y. Youngsheng, Z. Ying and H. DeFu (2016). Isomers and Their Metabolites of Endosulfan Induced Cytotoxicity and Oxidative Damage in SH-SY5Y Cells. Environ Toxicol 31: 496-504.

Fendick, E. A., E. Mather-Mihaich, K. A. Houck, M. B. St Clair, J. B. Faust, C. H. Rockwell and M. Owens (1990). Ecological toxicology and human health effects of heptachlor. Rev Environ Contam Toxicol 111: 61-142.

Gannon, N. and J. H. Bigger (1958a). The conversion of aldrin and heptachlor to their epoxides in soil. J Econ Entom 51: 1-2.

Gannon, N. and G. C. Decker (1958b). The conversion of heptachlor to its epoxide on plants. J Econ Entom 51: 3-7.

Gkaleni, N. (2021). Studies of Bacterial and Insect Cytochromes P450 in Degradation of Pesticides. M. Sc., Simon Fraser University.

Green, M. T., J. H. Dawson and H. B. Gray (2004). Oxoiron(IV) in chloroperoxidase compound II is basic: Implications for P450 chemistry. Science 304(5677): 1653-1656.

Guo, Y., A. Baschieri, F. Mollica, L. Valgimigli, J. Cedrowski, G. Litwinienko and R. Amorati (2021). Hydrogen Atom Transfer from HOO(.) to ortho-Quinones Explains the Antioxidant Activity of Polydopamine. Angew Chem Int Ed Engl 60(28): 15220-15224.

Harman-Fetcho, J. A., C. J. Hapeman, L. L. McConnell, T. L. Potter, C. P. Rice, A. M. Sadeghi, R. D. Smith, K. Bialek, K. A. Sefton, B. A. Schaffer and R. Curry (2005). Pesticide occurrence in selected South Florida canals and Biscayne Bay during high agricultural activity. J Agric Food Chem 53(15): 6040-6048.

Hirakawa, K., S. Oikawa, Y. Hiraku, I. Hirosawa and S. Kawanishi (2002). Catechol and Hydroquinone Have Different Redox Properties Responsible for Their Differential DNA-Damaging Ability. Chem Res Toxicol 15(1): 76-82.

Hiruma, Y., M. A. Hass, Y. Kikui, W. M. Liu, B. Olmez, S. P. Skinner, A. Blok, A. Kloosterman, H. Koteishi, F. Lohr, H. Schwalbe, M. Nojiri and M. Ubbink (2013). The structure of the cytochrome p450cam-putidaredoxin complex determined by paramagnetic NMR spectroscopy and crystallography. J Mol Biol 425(22): 4353-4365.

Hussain, S., M. Arshad, M. Saleem and A. Khalid (2007). Biodegradation of alpha- and beta-endosulfan by soil bacteria. Biodegradation 18(6): 731-740.

Hussain, S., M. Arshad, M. Saleem and Z. A. Zahir (2007). Screening of soil fungi for in vitro degradation of endosulfan. World Journal of Microbiology & Biotechnology 23(7): 939-945.

Jimenez-Torres, C., I. Ortiz, P. San-Martin and R. I. Hernandez-Herrera (2016). Biodegradation of malathion, alpha- and beta-endosulfan by bacterial strains isolated from agricultural soil in Veracruz, Mexico. J Environ Sci Health B 51(12): 853-859.

Kammoonah, S., B. Prasad, P. Balaraman, H. Mundhada, U. Schwaneberg and E. Plettner (2018). Selecting of a Cytochrome P450cam SeSaM Library with 3-Chloroindole and Endosulfan – Identification of Mutants That Dehalogenate 3-Chloroindole. BBA Proteins Proteom. 1866: 68-79.

Kataoka, R., K. Takagi and F. Sakakibara (2010). A new endosulfan-degrading fungus, Mortierella species, isolated from a soil contaminated with organochlorine pesticides. Journal of Pesticide Science 35(3): 326-332.

Kataoka, R., K. Takagi and F. Sakakibara (2011). Biodegradation of endosulfan by Mortieralla sp. strain W8 in soil: Influence of different substrates on biodegradation. Chemosphere 85(3): 548-552.

Kelly, B. C., M. G. Ikonomou, J. D. Blair, A. E. Morin and F. A. Gobas (2007). Food web-specific biomagnification of persistent organic pollutants. Science 317(5835): 236-239.

Kullman, S. W. and F. Matsumura (1996). Metabolic pathways utilized by Phanerochaete chrysosporium for degradation of the cyclodiene pesticide endosulfan. Appl Environ Microbiol 62(2): 593-600.

Kwon, G. S., J. E. Kim, T. K. Kim, H. Y. Sohn, S. C. Koh, K. S. Shin and D. G. Kim (2002). Klebsiella pneumoniae KE-1 degrades endosulfan without formation of the toxic metabolite, endosulfan sulfate. Fems Microbiology Letters 215(2): 255-259.

Labute, P. (2008). The Generalized Born/Volume Integral Implicit Solvent Model: Estimation of the Free Energy of Hydration Using London Dispersion Instead of Atomic Surface Area. J. Comput. Chem. 29: 1693-1698.

Labute, P. (2009). Protonate3D: assignment of ionization states and hydrogen coordinates to macromolecular structures. Proteins 75(1): 187-205.

Lee, Y. T., R. F. Wilson, I. Rupniewski and D. B. Goodin (2010). $P450_{cam}$ Visits an Open Conformation in the Absence of Substrate. Biochemistry 49(16): 3412-3419.

Lefever, M. R. and L. P. Wackett (1994). Oxidation of low molecular weight chloroalkanes by cytochrome P450CAM. Biochem Biophys Res Commun 201(1): 373-378.

Li, S. and L. P. Wackett (1993). Reductive dehalogenation by cytochrome P450CAM: substrate binding and catalysis. Biochemistry 32(36): 9355-9361.

Liebler, D. C. and F. P. Guengerich (1983). Olefin oxidation by cytochrome P-450: evidence for group migration in catalytic intermediates formed with vinylidene chloride and trans-1-phenyl-1-butene. Biochemistry 22(24): 5482-5489.

Logan, M. S., L. M. Newman, C. A. Schanke and L. P. Wackett (1993). Cosubstrate effects in reductive dehalogenation by Pseudomonas putida G786 expressing cytochrome P-450CAM. Biodegradation 4(1): 39-50.

Loida, P. J. and S. G. Sligar (1993). Molecular Recognition in Cytochrome P-450: Mechanism for the Control of Uncoupling Reactions. Biochemistry 32: 11530-11538.

Luek, J. L., R. M. Dickhut, M. A. Cochran, R. L. Falconer and H. Kylin (2017). Persistent organic pollutants in the Atlantic and southern oceans and oceanic atmosphere. Sci Total Environ 583: 64-71.

Lülsdorf, N., L. Vojcic, H. Hellmuth, T. T. Weber, N. Mussmann, R. Martinez and U. Schwaneberg (2015). A first continuous 4-aminoantipyrine (4-AAP)-based screening system for directed esterase evolution. Appl Microbiol Biotechnol 99(12): 5237-5246.

Miles, J. R., C. M. Tu and C. R. Harris (1969). Metabolism of heptachlor and its degradation products by soil microorganism. J Econ Entomol 62(6): 1334-1338.

Miles, J. R., C. M. Tu and C. R. Harris (1971). Degradation of heptachlor epoxide and heptachlor by a mixed culture of soil microorganisms. J Econ Entomol 64(4): 839-841.

Mukherjee, I. and A. Mittal (2005). Bioremediation of Endosulfan Using Aspergillus Terreus and Cladosporium Oxysporum. Bull Environ Contam Toxicol 75: 1034-1040.

Myers, W. K., Y. T. Lee, R. D. Britt and D. B. Goodin (2013). The Conformation of P450cam in Complex with Putidaredoxin Is Dependent on Oxidation State. J Am Chem Soc 135: 11732-11735.

Ortiz de Montellano, P. R. (2015). Substrate Oxidation by Cytochrome P450 Enzymes. Cytochrome P450: Structure, Mechanism, and Biochemistry P. R. Ortiz de Montellano. Switzerland, Springer 111-176.

Pochapsky, S. S., T. C. Pochapsky and J. W. Wei (2003). A Model for Effector Activity in a Highly Specific Biological Electron Transfer Complex: The Cytochrome P450cam−Putidaredoxin Couple. Biochemistry 42: 5649-5656.

Pochapsky, T. C. and S. S. Pochapsky (2019). What Your Crystal Structure Will Not Tell You about Enzyme Function. Acc Chem Res 52: 1409-1418.

Poulos, T. L., B. C. Finzel, I. C. Gunsalus, G. C. Wagner and J. Kraut (1985). The 2.6-A crystal structure of Pseudomonas putida cytochrome P-450. J Biol Chem 260(30): 16122-16130.

Pozo, K., T. Harner, F. Wania, D. C. G. Muir, K. C. Jones and L. A. Barrie (2006). Toward a global network for persistent organic pollutants in air: Results from the GAPS study. Environ Sci Technol 40(16): 4867-4873.

Prasad, B. (2013). The Borneol Cycle of Cytochrome $P450_{cam}$ and Evolution of the Enzyme for New Applications. Ph. D., Simon Fraser University.

Prasad, B., A. Rojubally and E. Plettner (2011). Identification of camphor oxidation and reduction products in Pseudomonas putida: new activity of the cytochrome $P450_{cam}$ system. J Chem Ecol **37**(6): 657-667.

Purnomo, A. S., S. R. Putra, K. Shimizu and R. Kondo (2014). Biodegradation of heptachlor and heptachlor epoxide-contaminated soils by white-rot fungal inocula. Environ Sci Pollut Res 21(19): 11305-11312.

Qiu, L., H. Wang and X. Wang (2018). Heptachlor degradation characteristics of a novel strain and its application. Water Sci Technol 77: 2113-2122.

Rehman, A. (2021). Cytochrome P450cam (CYP101A1) Mutants to Study the Dehalogenation of Endosulfan: A Persistent Organic Pollutant, and Oxidation of β-Phellandrene: A Monoterpene. Ph. D., Simon Fraser University.

Schmidt, W. F., S. Bilboulian, C. P. Rice, J. C. Fettinger, L. L. McConnell and C. J. Hapeman (2001). Thermodynamic, spectroscopic, and computational evidence for the irreversible conversion of beta- to alpha-endosulfan. J Agric Food Chem 49(11): 5372-5376.

Schmidt, W. F., C. J. Hapeman, J. C. Fettinger, C. P. Rice and S. Bilboulian (1997). Structure and Asymmetry in the Isomeric Conversion of β- to α-Endosulfan. J Agric Food Chem 45: 1023-1026.

Schulze, H., G. Hui Bon Hoa, V. Helms, R. C. Wade and C. Jung (1996). Structural Changes in Cytochrome P-450cam Effected by the Binding of the Enantiomers (1R)-Camphor and (1S)-Camphor. Biochemistry 35: 14127-14138.

Shen, L. and F. Wania (2005). Compilation, evaluation, and selection of physical-chemical property data for organochlorine pesticides. Journal of Chemical and Engineering Data 50(3): 742-768.

Shen, L., F. Wania, Y. D. Lei, C. Teixeira, D. C. Muir and T. F. Bidleman (2005). Atmospheric distribution and long-range transport behavior of organochlorine pesticides in North America. Environ Sci Technol 39(2): 409-420.

Siddique, T., B. C. Okeke, M. Arshad and W. T. Frankenberger (2003). Enrichment and Isolation of Endosulfan-Degrading Microorganisms. J. Environ. Qual. 32: 47-54.

Skinner, S. P., A. H. Follmer, M. Ubbink, T. L. Poulos, J. J. Houwing-Duistermaat and F. Paci (2021). Partial Opening of Cytochrome P450cam (CYP101A1) Is Driven by Allostery and Putidaredoxin Binding. Biochemistry 60: 2932-2942.

Stanley, J., K. Sah, S. K. Jain, J. C. Bhatt and S. N. Sushil (2015). Evaluation of pesticide toxicity at their field recommended doses to honeybees, Apis cerana and A-mellifera through laboratory, semi-field and field studies. Chemosphere 119: 668-674.

Sutherland, T. D., I. Horne, R. L. Harcourt, R. J. Russell and J. G. Oakeshott (2002). Isolation and characterization of a Mycobacterium strain that metabolizes the insecticide endosulfan. J Appl Microbiol 93(3): 380-389.

Sutherland, T. D., I. Horne, M. J. Lacey, R. L. Harcourt, R. J. Russell and J. G. Oakeshott (2000). Enrichment of an endosulfan-degrading mixed bacterial culture. Appl Environ Microbiol 66(7): 2822-2828.

Sutherland, T. D., I. Horne, R. J. Russell and J. G. Oakeshott (2002). Gene cloning and molecular characterization of a two-enzyme system catalyzing the oxidative detoxification of beta-endosulfan. Appl Environ Microbiol 68(12): 6237-6245.

Sutherland, T. D., K. M. Weir, M. J. Lacey, I. Horne, R. J. Russell and J. G. Oakeshott (2002). Enrichment of a microbial culture capable of degrading endosulphate, the toxic metabolite of endosulfan. J Appl Microbiol 92(3): 541-548.

Tripathi, S., H. Li and T. L. Poulos (2013). Structural Basis for Effector Control and Redox Partner Recognition in Cytochrome P450. Science 340(6137): 1227-1230.

Unno, M., J. F. Christian, D. E. Benson, N. C. Gerber, S. G. Sligar and P. M. Champion (1997). Resonance Raman Investigations of Cytochrome $P450_{cam}$ Complexed with Putidaredoxin. J Am Chem Soc 119: 6614-6620.

Volkamer, A., A. Griewel, T. Grombacher and M. Rarey (2010). Analyzing the topology of active sites: on the prediction of pockets and subpockets. J Chem Inf Model **50**(11): 2041-2052.

Wackett, L. P. (1995). Recruitment of co-metabolic enzymes for environmental detoxification of organohalides. Environ Health Perspect 103 Suppl 5: 45-48.

Wackett, L. P., M. J. Sadowsky, L. M. Newman, H. G. Hur and S. Li (1994). Metabolism of polyhalogenated compounds by a genetically engineered bacterium. Nature 368(6472): 627-629.

Walse, S. S., G. I. Scott and J. L. Ferry (2003). Stereoselective degradation of aqueous endosulfan in modular estuarine mesocosms: formation of endosulfan gamma-hydroxycarboxylate. J Environ Monit 5(3): 373-379.

Wan, M. T., J. N. Kuo, B. McPherson and J. Pasternak (2006). Agricultural pesticide residues in farm ditches of the Lower Fraser Valley, British Columbia, Canada. J Environ Sci Health B 41(5): 647-669.

Wauchope, R. D., T. M. Buttler, A. G. Hornsby, P. W. M. Augustijn-Beckers and J. P. Burt (1992). The SCS/ARS/CES Pesticide Properties Database for Environmental Decision-Making. Reviews of Environmental Contamination and Toxicology: Continuation of Residue Reviews G. W. Ware. New York, Springer**:** 1-155.

Weber, J., C. J. Halsall, D. C. G. Muir, C. Teixera, D. A. Burniston, W. M. J. Strachan, H. Hung, N. Mackay, D. Arnold and H. Kylin (2006). Endosulfan and γ-HCH in the Arctic: An Assessment of Surface Seawater Concentrations and Air−Sea Exchange. Environ Sci Technol 40: 7570-7576.

Wojciechowski, M. and B. Lesyng (2004). Generalized Born Model: Analysis, Refinement, and Applications to Proteins. J. Phys. Chem. B 108: 18368-18376.

Wong, T. S., N. Wu, D. Roccatano, M. Zacharias and U. Schwaneberg (2005). Sensitive assay for laboratory evolution of hydroxylases toward aromatic and heterocyclic compounds. J Biomol Screen 10(3): 246-252.

Xiao, P., T. Mori, I. Kamei and R. Kondo (2011). Metabolism of organochlorine pesticide heptachlor and its metabolite heptachlor epoxide by white rot fungi, belonging to genus Phlebia. FEMS Microbiol. Lett. 314: 140-146.

Zeng, Z., L. Tian, Z. Li, L. Jia, X. Zhang, M. Xia and Y. Hu (2015). Whole-Cell Method for Phenol Detection Based on the Color Reaction of Phenol with 4-Aminoantipyrine Catalyzed by CotA Laccase on Endospore Surfaces. Biosens Bioelectron 69: 162-166.